РОССИЙСКАЯ АКАДЕМИЯ НАУК

Физический институт имени П.Н.Лебедева

ФИАН

ПРЕПРИНТ

1

V.D. ZVORYKIN, N.V. DIDENKO, A.A. IONIN, I.V. KHOLIN, A.V. KONYASHCHENKO, O.N. KROKHIN, A.O. LEVCHENKO, A.O. MAVRITSKII, G.A. MESYATS, A.G. MOLCHANOV, M.A. ROGULEV, L.V. SELEZNEV, D.V. SINITSYN, S.Yu. TENYAKOV, N.N. USTINOVSKII, D.A. ZAYARNYI

HYBRID Ti:SAPPHIRE/KrF LASER FACILITY GARPUN-MTW FOR COMBINED SUBPICOSECOND/NANOSECOND LASER-MATTER INTERACTION

МОСКВА 2007

Hybrid Ti:Sapphire/KrF laser facility GARPUN-MTW for combined subpicosecond/nanosecond laser-matter interaction

**V.D. Zvorykin [1], N.V. Didenko [2], A.A. Ionin [1], I.V. Kholin [1]
A.V. Konyashchenko [1, 2], O.N. Krokhin [1], A.O. Levchenko [1],
A.O. Mavritskii [2], G.A. Mesyats [1], A.G. Molchanov [1], M.A. Rogulev [1],
L.V. Seleznev [1], D.V. Sinitsyn [1], S.Yu. Tenyakov [2],
N.N. Ustinovskii [1], D.A. Zayarnyi [1]**

[1] P.N. Lebedev Physical Institute, Russian Academy of Sciences,
Leninsky Prospect 53, 119991 Moscow, Russia
[2] Avesta Project Ltd., Solnechnaya st. 12, 142190 Troitsk, Moscow region, Russia

Corresponding author: Dr. Vladimir D. Zvorykin
Russian Academy of Sciences, P.N. Lebedev Physical Institute
Leninsky pr.53, 119991 Moscow, Russia
Fax: +7 (495) 132 0425, Tel: +7 (495) 132 6739, e-mail: zvorykin@sci.lebedev.ru

Number of pages: 46; **Tables:** 2; **Figures:** 28.

Гибридная Ti:Sapphire/KrF лазерная установка ГАРПУН-MTW для взаимодействия комбинированных субпикосекундных/наносекундных лазерных импульсов с веществом

**В.Д. Зворыкин [1], Н.В. Диденко [2], А.А. Ионин [1], И.В. Холин [1]
А.В. Конященко [1, 2], О.Н. Крохин [1], А.О. Левченко [1],
А.О. Маврицкий [2], Г.А. Месяц [1], А.Г. Молчанов [1], М.А. Рогулев [1],
Л.В. Селезнев [1], Д.В. Синицын [1], С.Ю. Теняков [2],
Н.Н. Устиновский [1], Д.А. Заярный [1]**

[1] Физический институт им. П.Н. Лебедева Российской Академии Наук,
Ленинский проспект 53, 119991 Москва, Россия
[2] Компания Авеста, Солнечная улица 12, 142190 Троицк, Московская область, Россия

Автор для переписки: Владимир Д. Зворыкин
Российская Академия Наук, Физический институт им. П.Н. Лебедева
Ленинский проспект, 119991 Москва, Россия
Факс: +7 (495) 132 0425, Тел: +7 (495) 132 6739, e-mail: zvorykin@sci.lebedev.ru

Число страниц: 46; **таблиц:** 2; **рисунков:** 28.

Abstract. The first stage of Petawatt Excimer Laser Project started at P.N. Lebedev Physical Institute implements a development of multiterawatt hybrid GARPUN-MTW laser facility for generation of ultra-high intensity subpicosecond UV laser pulses. Under this Project, a multi-stage e-beam-pumped 100-J, 100-ns GARPUN KrF laser was up-graded with a femtosecond Ti:Sapphire front-end to produce combined subpicosecond/nanosecond laser pulses with variable time delay. Attractive possibility to amplify simultaneously short & long pulses in the same large-scale KrF amplifiers is analyzed with regard to the fast-ignition Inertial Confinement Fusion problem. Detailed description of hybrid laser system is presented with synchronized KrF and Ti:Sapphire master oscillators. Gain and absorption measurements at GARPUN amplifier, being compared with numerical simulations based on a quasi-stationary code, precede amplification of short pulses in large-aperture e-beam-pumped modules. Amplified spontaneous emission, which is responsible for the pre-pulse formation on a target, was also investigated: its acceptable level can be provided by properly choosing stage gain or loading the amplifiers by quasi-steady laser radiation. Fluorescence and transient absorption spectra of $Ar/Kr/F_2$ mixtures conventionally used in KrF amplifiers were recorded to find out the possibility for femtosecond pulse amplification at the broadband Kr_2F ($4^2\Gamma \rightarrow 1{,}2\ ^2\Gamma$) transition. Numerical simulations predict that 1.6 J can be obtained in a short pulse at hybrid GARPUN-MTW Ti:Sapphire / KrF laser facility combined with several tens of joules in nanosecond pulse.

Keywords: e-beam-pumped high-power KrF laser system with short-pulse Ti:Sapphire front-end, generation of ultra-high intensity laser pulses.

1. Overview of ultrahigh-intensity short-pulse generation: From multi-terawatt excimer systems to petawatt solid-state lasers

Short femtosecond or picosecond pulses with ultra-high intensities (UHI) $>10^{18}$ W/cm^2, which can be reached in a focused beam of TW lasers are of a great importance for many fundamental fields and practical applications. Among them there are generation of high-order short-wavelength harmonics and attosecond pulses of X-ray radiation, acceleration of electrons and protons over GeV energies, investigations in high-energy-density physics of relativistic plasma, laboratory modeling of astrophysical phenomena, isochoric heating of solid matter for strong shock wave generation and equation of state studies, development of coherent and non-coherent soft X-ray sources for radiography, microlithography and biomedical applications, etc. In the fast-ignition concept (Basov *et al.*, 1992; Tabak *et al.*, 1994), which is considered today as the most promising way for the Inertial Confinement Fusion (ICF), thermonuclear reaction is implemented in two steps: a conventional "long" nanosecond laser pulse (typically $\tau_{long} \sim 5$ ns) produces an implosion of a shell pellet and the following short UHI laser pulse ($\tau_{sh} \sim 1 \div 20$ ps) heats and ignites the collapsed fuel before it begins to expand. For a novel target design where 0.5-PW, 0.6-ps UHI pulse was delivered through a cone to the center of a spherical target preliminary compressed by 2.5-kJ, 1.2-ns pulse, 1000-fold increase in the neutron yield and 20÷30 % efficiency of UHI pulse coupling to the plasma energy were demonstrated by Kodama *et al.* (2002). If the efficiency would be the same for UHI pulse of 10÷20-ps duration, equal to expanding time of the compressed region, the total energy of the main ICF laser driver can be significantly reduced down to a few hundred kilojoules. For comparison, 1.8 MJ is projected for the National Ignition Facility (NIF) at LLNL, USA (Moses *et al.*, 2006) and Laser Mega Joule (LMJ) at CEA/CESTA Laboratory, France (Bigot, 2006) in the conventional ICF scheme.

The output laser power achievable in multi-stage master oscillator – power amplifier (MOPA) schemes with direct amplification of UHI pulses is mainly restricted by non-linear processes in amplifiers. Until chirped pulse amplification (CPA) scheme was developed (Strickland & Mourou, 1985; Pessot *et al.*, 1987) excimer laser systems using gaseous gain medium with essentially low non-linear refractive index were the only available to produce UHI pulses regardless their obvious disadvantage – saturation energy density $Q_s = \frac{h\nu}{\sigma} \cong 2$ mJ/cm^2 ($h\nu$=5 eV, the energy of quantum, σ =2.5·10^{-16} cm^2, induced emission cross section) being three orders of magnitude less than for solid-state lasers. As a result, large apertures are required for excimer amplifiers to obtain output power high enough. This is achievable with e-beam pumping technique. Another difference in comparison with solid-state lasers is short lifetime of the upper laser level. For KrF (B→X) laser transition, radiative lifetime is τ_r= 6.5 ns; collisional quenching reduces it to τ_c ~ 2 ns. As pumping time τ_p is significantly longer (for discharge-pumped excimer lasers minimum τ_p ~15-20 ns, whereas for e-beam-pumped ones, τ_p = 100÷500 ns), a multi-pass (Watanabe *et al.*, 1990), multi-beam (or angular multiplexing) (Ewing *et al.*, 1979; Lowenthal, *et al.*, 1981) or Raman summation scheme (Murray *et al.*, 1979; Hooker *et al.*, 1991; Shaw, 1991; Shaw *et al.*, 1993) are required to extract the stored energy efficiently.

Several approaches for UHI excimer laser systems (mainly KrF) were realized to-date (Schwarzenbach *et al.*, 1986; Szatmari *et al.*, 1987, 1988, 1992, 1996; Glownia *et al.*, 1988; Barr *et al.*, 1988; Roberts *et al.*, 1988; Watanabe *et al.*, 1988, 1990; Endoh *et al.*, 1989; Taylor *et al.*, 1990; Almasi *et al.*, 1992, 1995; Bouma *et al.*, 1993; Szatmari, 1994; Divall *et al.*, 1996; Nabekawa *et al.*, 1996; Omenetto *et al.*, 1997; Shaw *et al.*, 1999; Nabekawa *et al.*, 2001; Owadano *et al.*, 1999, 2001; Bekesi *et al.*, 2002). Various schemes were used to generate seed femtosecond or picosecond pulses in hybrid dye/excimer laser systems (Szatmari *et al.*, 1987, 1988, 1992) or in stimulated scattering processes (Takahashi, 2003, 2005). The most promising approach utilizes Ti: Sapphire MOPA front-end to produce femtosecond pulses at 745-nm wavelength, which then are frequency-tripled into KrF (B→X) amplification band. Because of limited 2.5-nm bandwidth of this transition, the seed pulses shorter than ~ 50 fs are not necessary. The shortest pulse amplified in a discharge-pumped KrF laser was 60-fs long (Szatmari & Schafer, 1988). The highest output power up to 10 TW was achieved at Super-SPRITE KrF facility equipped with e-beam-pumped TITANIA amplifier with 60-cm-aperture (Divall *et al.*, 1996, Shaw *et al.*, 1999). The pulse with a peak power of 3–4 TW (>10 J, ~ 3 ps) was obtained after 60-cm-aperture final amplifier of Super-ASHURA facility with short-pulse generator of simpler design based on stimulated backward Brillouin scattering (Owadano *et al.*, 2001). In the laser-plasma interaction studies, it was combined with 100-J, 20-ns pulse. CPA amplification was also successfully used in KrF amplifiers (Ross *et al.*, 1994; Houliston *et al.*, 1994) although it was not so efficient as in solid-state lasers. Nevertheless, short-wavelength KrF lasers provide better capability in focusing radiation and reaching intensities as high as 10^{20} W/cm^2 (Szatmary, 1994; Divall *et al.*, 1996; Shaw *et al.*, 1999). Very high average powers up to 50 W for a train of femtosecond pulses were demonstrated in UV spectral range at repetitively operating hybrid laser system, which combined a Ti:Sapphire front-end and a multi-pass 200-Hz discharge-pumped amplifier (Nabekawa *et al.*, 2001).

As soon as a chirped pulse amplification (CPA) scheme was developed, owing to overcoming non-linear distortion due to stretching of short pulses up to hundred picosecond, successive amplification and recompressing to initial pulse width, solid-state laser systems surpassed excimer systems in output energy and peak power and, for the first time, achieved the PW level (Key *et al.*, 1998). Rapid progress in CPA technique in combination with optical parametric amplification (OPA) in non-linear crystals provides to-date most experimental means mentioned above. Using the CPA and OPA, additional to the main amplifier chains PW laser channels are constructed and projected at the largest ICF glass facilities NIF (LLNL, USA) (Freeman *et al.*, 2006), OMEGA (LLE, USA) (Kelly *et al.*, 2006), VULCAN (RAL, UK) (Hernandez-Gomez *et al.*, 2006), GEKKOXII (ILE, Japan) (Miyanaga *et al.*, 2006), LMJ (CEA/CESTA, France) (Bigot, 2006) etc.

2. KrF drivers in the fast-ignition ICF problem

In our opinion, future trends of UHI pulse generation in excimer laser systems stem from explicit benefits of KrF drivers for ICF. Investigations of both laser physics and laser-plasma interaction during two past decades at 0.1-10.0 kJ-class single-shot KrF facilities AURORA (LANL, USA) (Rosocha *et al.*, 1986, 1987; Harris *et al.*, 1993), NIKE (NRL, USA) (Obenschain *et al.*, 1996; Pawley *et al.*, 1997, 1999, Aglitskiy *et al.*, 2002;), SPRITE (RAL, UK) (Shaw *et al.*, 1993, 1999; Divall *et al.*, 1996), ASHURA (AIS&T, Japan) (Owadano *et al.*, 1989, 1993, 1999, 2001) and GARPUN (LPI, Russia) (Basov *et al.*, 1993; Zvorykin & Lebo, 1999; Zvorykin *et. al.*, 2001, 2004, 2006 a) and especially at rep-rate ELECTRA laser (NRL, USA) (Sethian *et al.*, 1998, 1999, 2003; Wolford *et al.*, 2006) have proved that e-beam-pumped KrF laser might be the best challenge for direct-drive ICF power plant. To satisfy physical and economical requirements, they should be scaled to output energies of 30-60 kJ per one module, operating all together with the total laser energy of ~2 MJ at rep-rate of 5 Hz and overall system efficiency of 7.5% (Svyatoslavsky *et al.*, 1992; Von Rosenberg, 1992; M.W. McGeoch *et al.*, 1997; Sethian *et al.*, 2003). Only diode-pumped solid-state (DPSS) laser seems to compete with KrF laser as a future reactor driver (Lindl *et al.*, 2003; Bibeau *et al.*, 2006; Kawashima *et al.*, 2006).

An important feature of KrF driver for the fast ignition application is very fast population inversion recovery time τ_c ~ 2 ns of the gain medium. This means amplification of a short UHI laser pulse ($\tau_{sh} << \tau_c$) can be repeated each 2 ns and it hardly affects subsequent amplification of long pulses ($\tau_{long} \geq \tau_c$). Therefore it will be very attractive to amplify both long laser pulses for pellet compression and UHI short pulses for fuel ignition in the same large-scale e-beam-pumped amplifiers (Fig. 1) (Zvorykin *et al.*, 1997). On the other hand, amplification of a quasi-continuous train of long pulses in angular multiplexing layout would deplete the population inversion and control amplified spontaneous emission (ASE), which is rather high due to a short radiation lifetime.

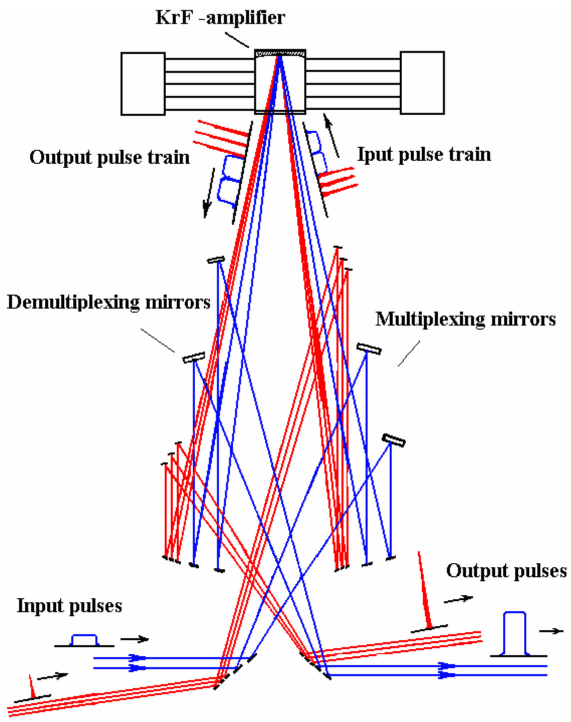

Fig. 1. Principle of simultaneous angular multiplication of short & long pulses in KrF amplifiers.

McGeogh *et al.* (1997) proposed 2-MJ laser fusion KrF facility consisting of 68-kJ modules of 2-m^2 aperture each. All 32 modules with a total aperture of 64 m^2 are combined in 16 angular-multiplexed 136-kJ beamlines. The optimal energy density for a short pulse amplification corresponding to the highest extraction efficiency from a unit of amplifier aperture is $Q_{opt} = Q_s \ln(g_0 / \alpha_{ns})$ = 5÷6 mJ/cm^2 (Tilleman & Jacobs, 1987), where the ratio of small-signal gain coefficient to nonsaturable absorption coefficient g_0 / α_{ns}=10÷20 slightly varies with pumping conditions (Molchanov, 1988). Therefore, the total energy available for a single short-pulse at the output of all amplifiers would be up to 4 kJ. By means of N-fold angular multiplexing, the energy could be increased up to required level which takes time of about $t_{sh} = N\tau_c$. For example, for N =25, the total energy in short pulse is 100 kJ and t_{sh} =50 ns, which is significantly less then projected pumping time τ_p =250 ns. Then the rest of time $t_{long} = \tau_p - t_{sh}$ =200 ns might be used for amplification of long pulses.

In another performance, a train of short pulses might be amplified against the background of loading the amplifier by a train of long pulses. For a quasi-stationary amplification, the optimal intensity $I_{opt} = I_s \left[(g_0 / \alpha_{ns})^{1/2} - 1 \right]$, where $I_s = Q_s / \tau_c = \dfrac{h\nu}{\sigma\tau_c}$ = 1÷3 MW/cm^2, saturation intensity, decreases the gain-to-loss ratio to $g / \alpha_{ns} = (g_0 / \alpha_{ns})^{1/2}$ This gives for a short pulse $Q_{opt} = \frac{1}{2} Q_s \ln(g_0 / \alpha_{ns})$, which is one-half of that for amplification of short pulses alone.

Note that for decoding of short pulses to required duration τ_{sh} ~ 10 ps, the lengths in angular multiplexer should be adjusted with an accuracy of 3 mm, which seems to be attainable. By using an appropriate mismatch in the beam lengths, it is possible to introduce required shaping into a short pulse reaching a target.

Investigation of amplification of both long and short laser pulses in KrF amplifiers is the first stage of Petawatt Excimer Laser Project (PEL Project) started at P.N. Lebedev Physical Institute (Zvorykin, 2006 b). Its goal is to verify the above-described fast-ignition ICF concept utilizing KrF drivers for simultaneous amplification of short & long laser pulses.

Another attractive possibility for amplification of short pulses is to use the $4^2\Gamma \rightarrow 1{,}2\ ^2\Gamma$ transition of Kr_2F trimer molecule. Such molecules are formed along with dimer KrF molecules in typical $Ar/Kr/F_2$ working gas mixtures during KrF laser pumping (Molchanov, 2006). They have a broad bandwidth of 80 nm (it corresponds to spectrally limited pulse of ~10 fs) around ~ 400 nm, long lifetime of the upper level of 180 ns, and high saturation energy Q_s ~ 0.2 J/cm^2 (Quigley & Hughes, 1978). All these enable one to accumulate population inversion during pumping time and to extract more power from the amplifier in a short pulse with lower ASE background. So far, only free-running oscillation was observed at Kr_2F being strongly affected by absorption in the gain medium (Tittel *et al.*, 1980).

3. GARPUN laser facility

Layout of the hybrid Ti:Sapphire/KrF multiterawatt laser facility GARPUN-MTW for amplification of combined subpicosecond/nanosecond pulses is shown schematically in Fig. 2. A newly developed Ti: Sapphire front-end "START-248 M" is currently upgrading the GARPUN KrF laser facility (Zvorykin & Lebo, 1999; Zvorykin *et al.*, 2001).

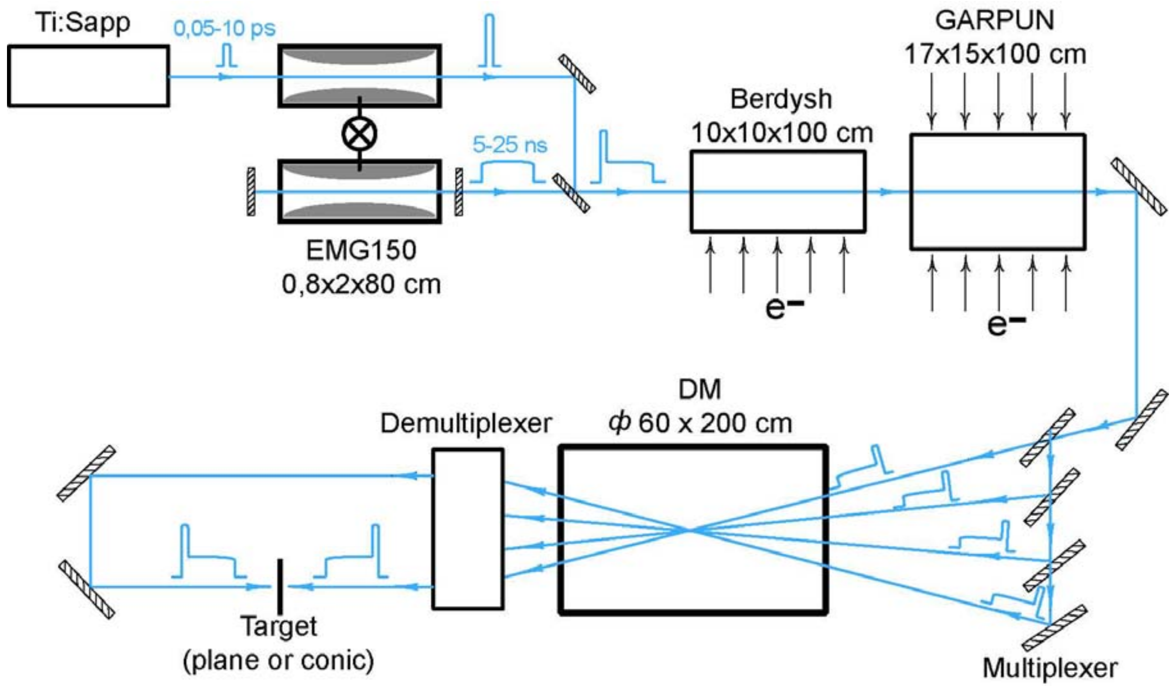

Fig. 2. Layout of hybrid Ti:Sapphire/KrF laser facility GARPUN MTW for amplification of combined subpicosecond/nanosecond pulses.

The final large-aperture GARPUN amplifier module (Fig. 3) operates since 1990 and has generated about 8,000 shots with output energy of up to 100 J (Basov *et al.*, 1993;). It has an active volume dimensioned 16×18×100 cm pumped by two-side counter-propagating 350-keV, 60-kA (50 A/cm^2), 100-ns e-beams with magnetic field (~0.08 T) guiding (Fig. 4).

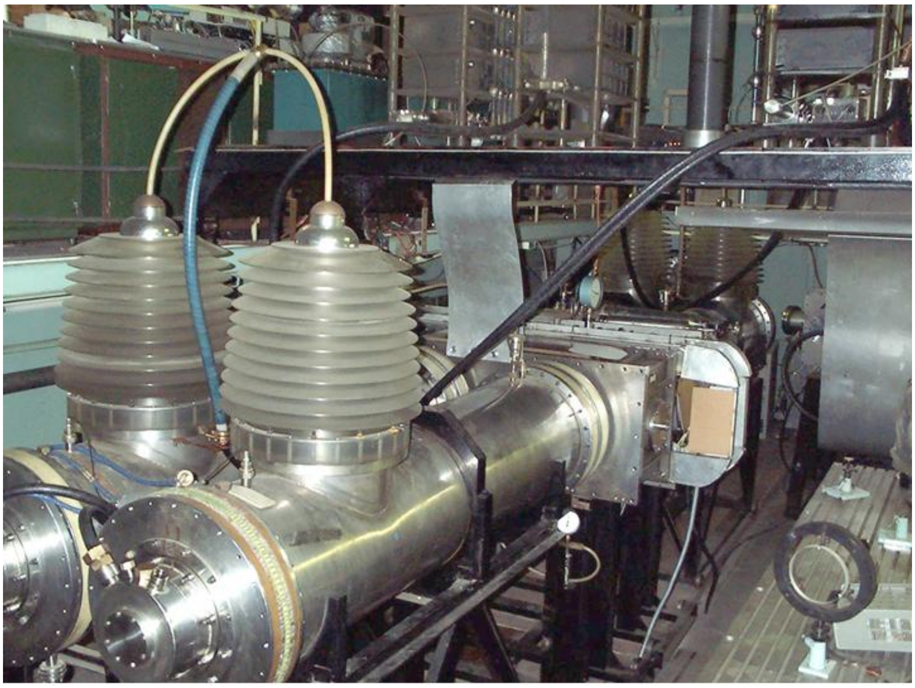

Fig. 3. Final e-beam-pumped amplifier of GARPUN KrF facility.

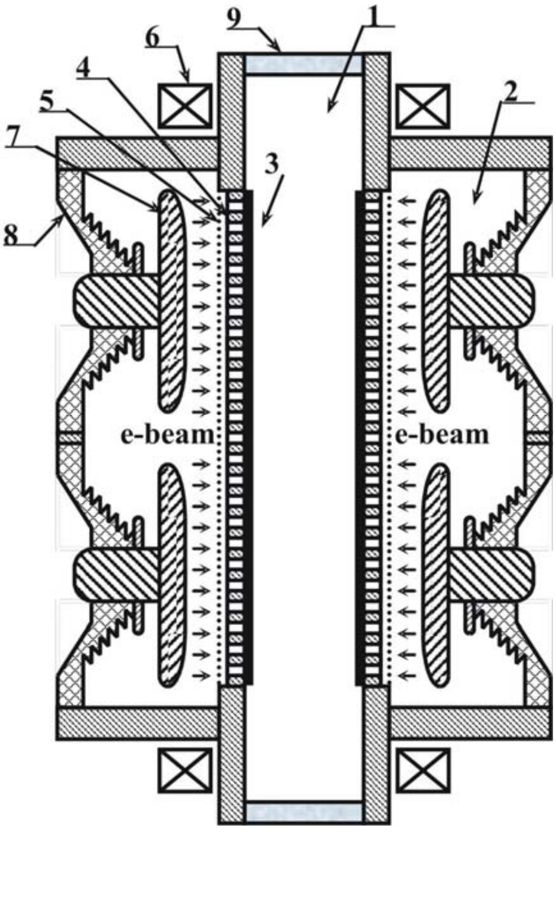

Fig. 4. Schematic layout of final GARPUN amplifier: (1) laser chamber; (2) vacuum diode; (3) foil window; (4) hibachi; (5) anode grid; (6) solenoid; (7) cathode; (8) bushing; (9) output window.

Another 10×10×110-cm BERDYSH module pumped by a single-side magnetic field-guided 350-keV, 50-kA (50 A/cm^2), 100-ns e-beam provides up to 25 J in free-running oscillation.

A high-voltage power supply of electron guns consists of two separate 7-stage Marx generators with 14 kJ (GARPUN) and 3.0 kJ (BERDYSH) energy storage at 500-kV pulsed voltage and five water-filled Blumlein pulse forming lines (PFLs) of 7.6 Ω wave impedance (Fig. 5), which supply pulses of ~350 kV voltage to four cathodes in GARPUN's vacuum diodes and one cathode in BERDYSH module. All PFLs are synchronized by means of laser-triggered switches. Those are fired by optical pulses, which are chipped off from the output of discharge-pumped master oscillator and brought into the switches by an optical system (Fig. 6).

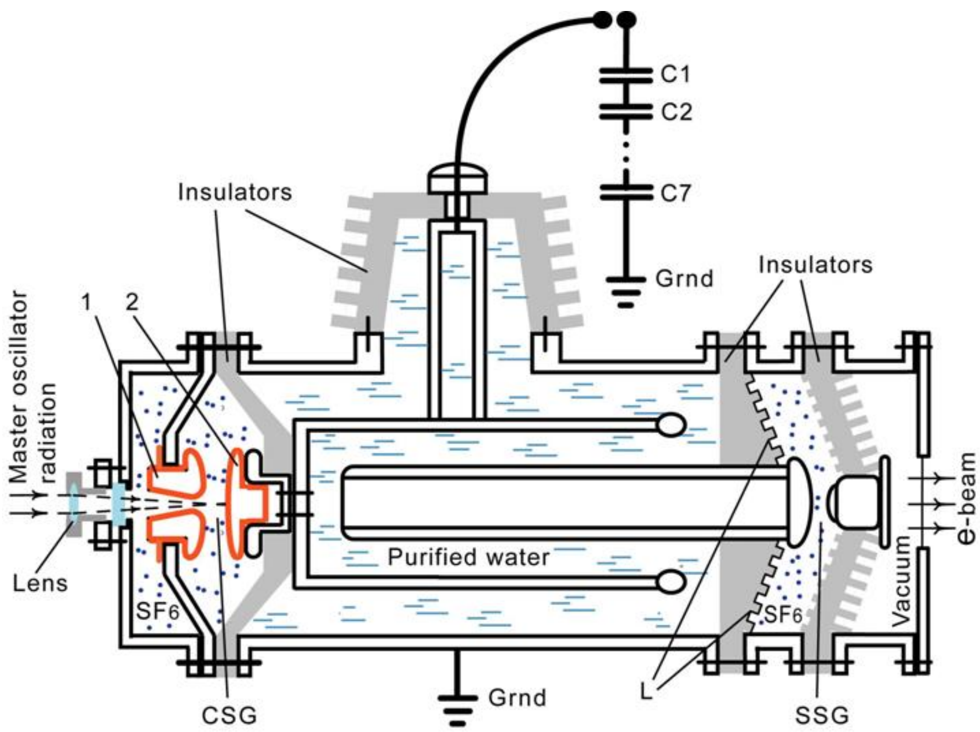

Fig. 5. Schematic layout of Blumlein PFL.

Excimer master oscillator is a commercial Lambda Physik EMG TMSC 150 laser with two separate discharge chambers synchronized by a common thyratron. It can be configured in different ways, for instance, as two independent oscillators or amplifiers or, being combined together in an injection-locked configuration, to produce narrow-band (~0.2 cm^{-1}) radiation tunable over emission band. At the present, two performances are considered: (i) the excimer master oscillator arranged in the narrow-band mode produces 20 ns, 0.2 mJ pulses, whereas a short pulse from Ti:Sapphire front-end is going roundabout to be combined subsequently with a long pulse; (ii) one of discharge chambers of the master oscillator operates in a conventional broad-band (~ 50 cm^{-1}) mode with approximately the same pulse energy and duration as in (i), while the other chamber serves as an amplifier for the short pulses (Fig. 2).

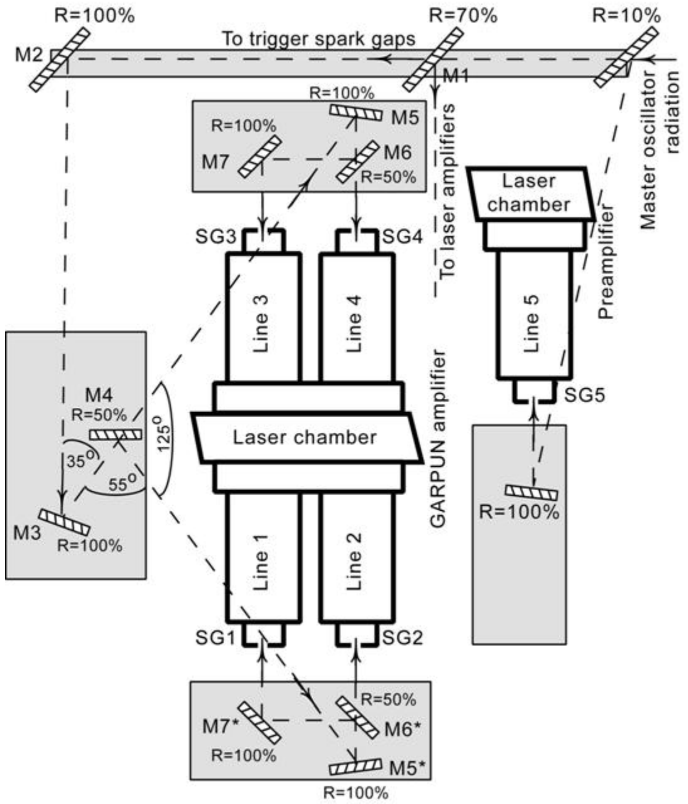

Fig. 6. Optical scheme for PFL's synchronization by master oscillator pulse.

Being combined together, short & long pulses are to be amplified successively in BERDYSH and GARPUN amplifiers. Large-scale DM amplifier (Fig. 2) will be implemented at the second stage of PEL Project. Schematic of this amplifier designed at High-Current Electronics Institute (Tomsk, Russia) is shown in Fig. 7. Its prototype operated with XeCl and produced up to 2 kJ output energy (Bugaev *et al.*, 2004). The specific pumping power ~0.3-0.5 MW cm^{-3} is provided by radially converging e-beams of 500÷600-keV energy and ~100 ns pulse duration. E-beams are generated in 12 vacuum diodes fed by a linear transformer. Optical diameter of 40÷60 cm and active length of 200 cm are assumed for DM amplifier.

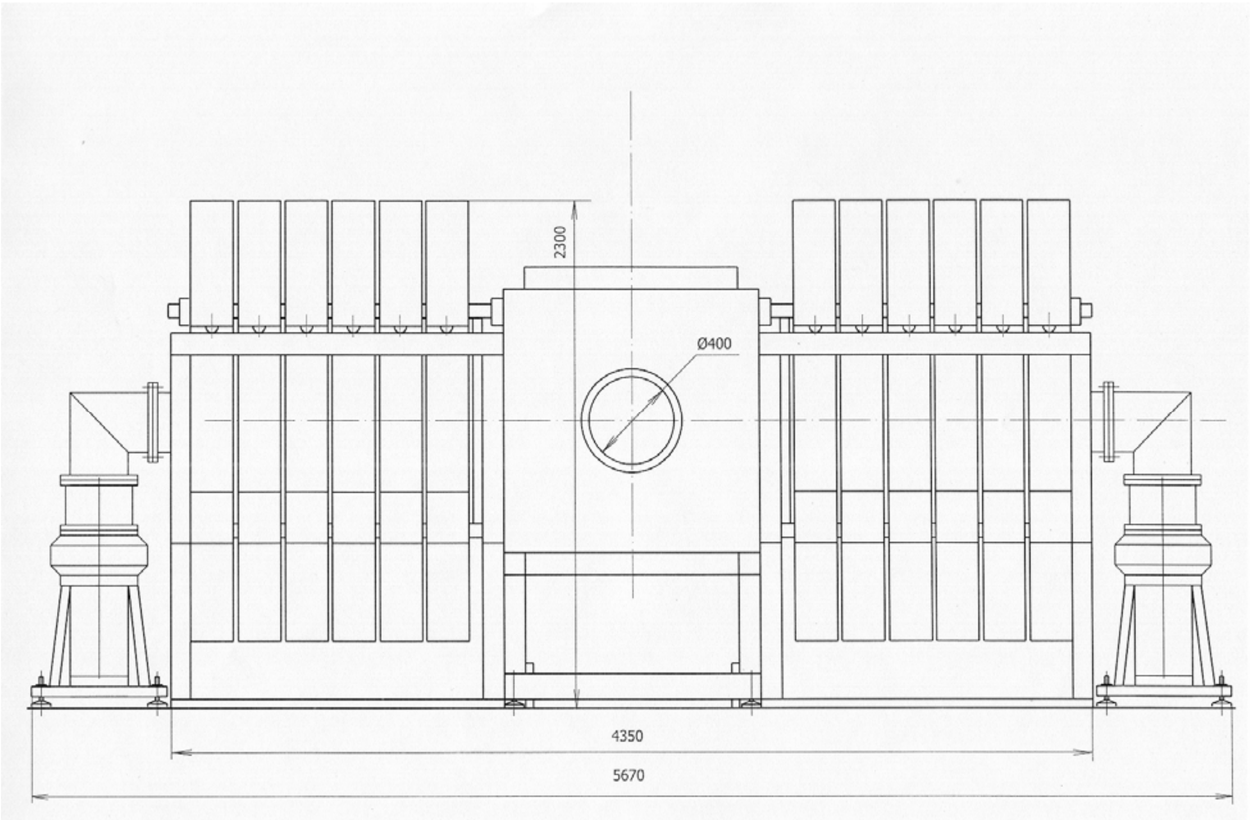

Fig. 7. Design of e-beam-pumped DM amplifier.

4. Ti:Sapphire front-end "START-248 M"

Ti: Sapphire front-end "START-248 M" was designed and constructed by Avesta Project Ltd. A block diagram of the laser is shown in Fig. 8.

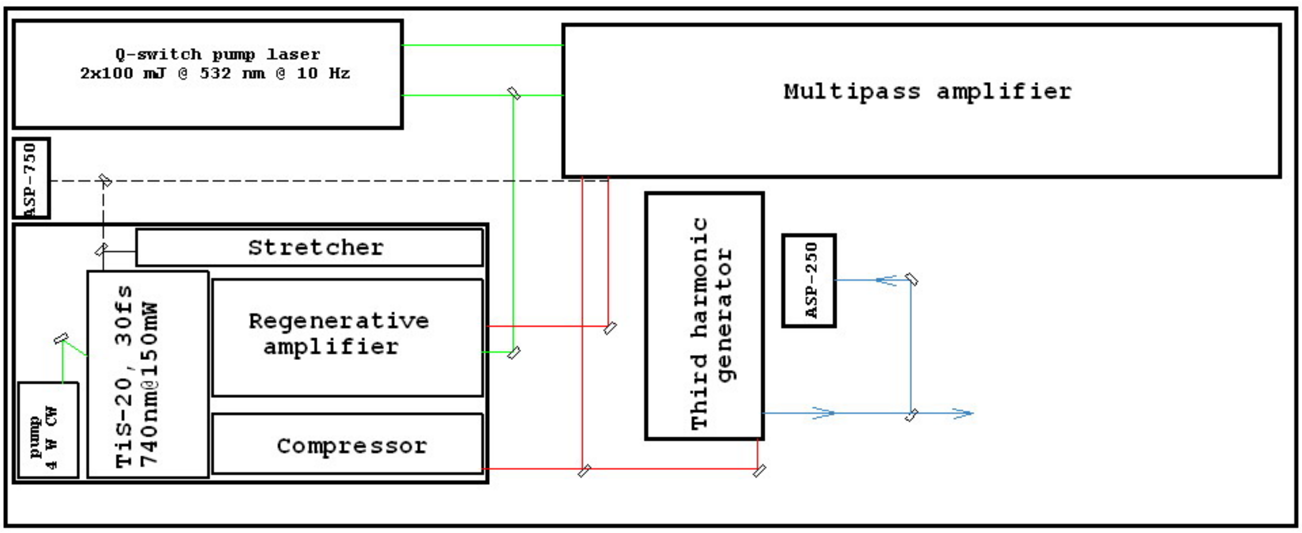

Fig. 8. Block diagram of Ti:Sapphire laser system.

Facility occupies a standard 120×300-cm^2 laboratory table. Ti:Sapphire oscillator TiS-20 with Laser Quantum 4-W CW Finesse 532 DPSS pumping laser (λ=532 nm), grating stretcher and compressor, and regenerative amplifier are enclosed in a common 60×110-cm^2 box. On the same table there are a multi-pass amplifier pumped by a pulsed two-channel Lotis-Tll Nd:YAG LS-2134 laser (2×100 mJ, 532 nm), 3-ω converter, ASP-750 and ASP-250 spectrometers for fundamental wavelength and the third harmonics, respectively.

The Kerr lens mode-locked oscillator TiS-20 when being pumped by 4-W CW radiation produces a continuous 80-MHz train of 30-fs pulses with nJ-level of energy and average power of 0.2 – 0.3 W. By choosing appropriate mirror's reflection, it is optimized to oscillate in a broad band of 28 – 32 nm centered at 740 nm. The folded cavity design is optimal for performance in minimal space (Fig. 9). The scheme incorporates pump beam routing flat mirror (Pm1), highly-reflecting wide spectral band beam folding mirrors (M1) –(M7), output coupler (OC), 5-mm long Ti:Sapphire Brewster angle crystal (TiS), lens for focusing the pump radiation (L), two prisms (P1 and P2) as dispersion control elements, slit (S) as spectrum-tuning element, and also alignment apertures.

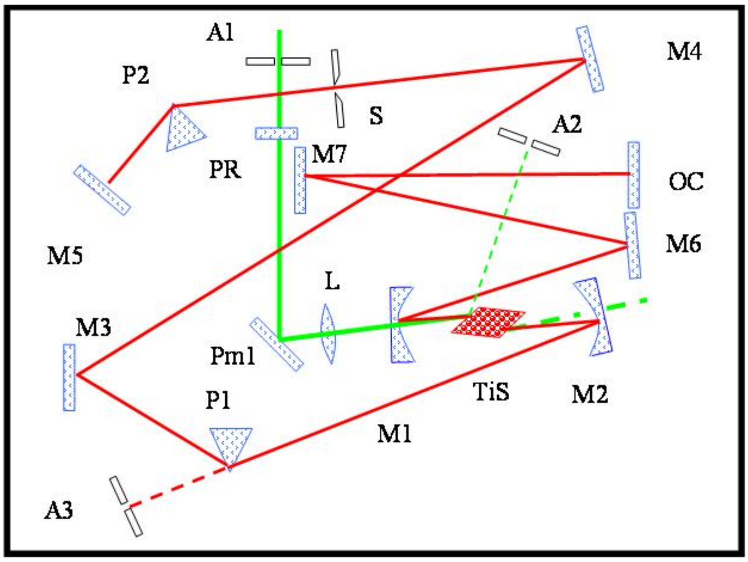

Fig. 9. Layout of TiS-20 oscillator: (TiS) Ti:Sapphire crystal; (M1) – (M7) HR mirrors; (Pm1) pump routing flat mirror; (OC) output coupler; (L) lens; (P1), (P2) prisms; (PR) polarization rotator; (S) spectrum-tuning slit; (A1) – (A3) aligning apertures.

Femtosecond pulses are stretched up to 200 ps in a double-pass all-reflected stretcher using a diffraction grating with 1200 grove/mm and 750-mm length mirror telescope. Afterwards they are forwarded through a Faraday isolator into regenerative amplifier where a single pulse is cut off of the train by a Pockels cell and amplified by ~10^6 times. The regenerative amplifier (Fig. 10) has Z-folded resonator cavity. One side of Ti:Sapphire crystal is cut at Brewster angle, another is HR coated to reflect both pumping and laser radiation. The prisms in the resonator serve for precise tuning of resonator into required spectral range and for compensation of the second- and third-order dispersions. The crystal is pumped by a fraction of the pulsed radiation produced in the first channel of Nd:YAG LS-2134 laser and passed through a polarizer (P2). Distribution of pumping radiation between the regenerative and multi-pass amplifiers can be varied with the help of polarization rotator (P1) and thin-film polarizer (P2).

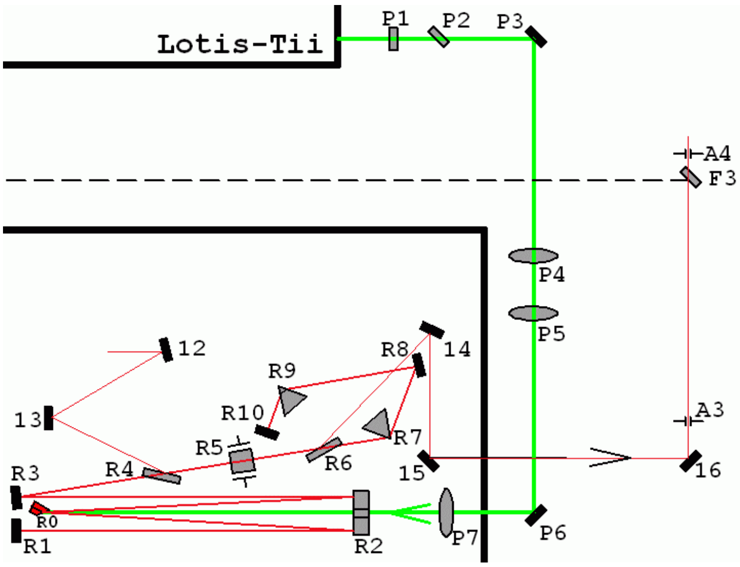

Fig. 10. Layout of regenerative amplifier. Resonator cavity optics: (R0) Ti:Sapphire crystal; (R1), (R3), (R10), HR flat mirrors; (R2) spherical mirror, (R4), (R6) thin-film polarizer; (R5) Pockels cell; (R7), (R9) prisms. Pump routing optics: (P1) polarization rotator; (P2) thin-film polarizer; (P3), (P6) HR flat mirrors; (P4), (P5) lens telescope. Laser routing optics: (12) – (16) HR flat mirrors.

Ejected from the regenerative amplifier ~1-mJ pulse is directed to the next amplifier stage (Fig. 11), in which, after 5 succeeding passages accomplish output energy of up to 15 mJ. Brewster angle crystal is pumped by the radiation of the first channel of Nd:YAG LS-2134 laser reflected by polarizer (P2). The pumping power in the crystal might be increased if necessary using the other channel of the pump laser with energy varied with the help of polarization rotator (P12) and polarizer (P13).

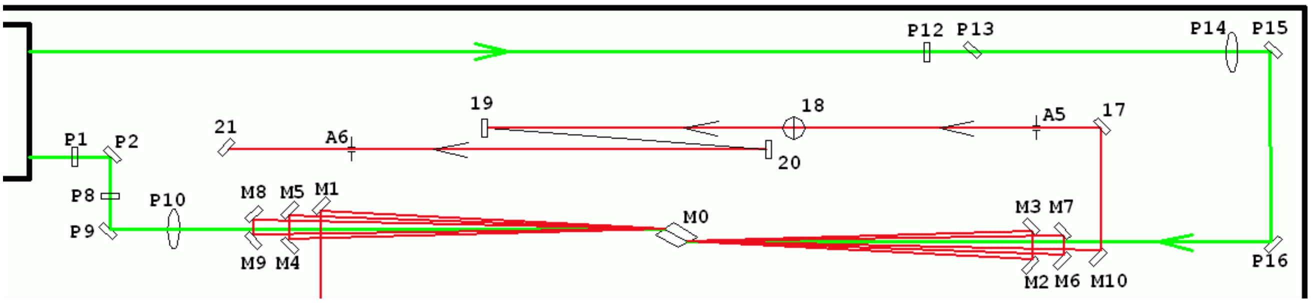

Fig. 11. Layout of multi-pass amplifier: (M0) Ti:Sapphire crystal; (M1) – (M10) HR mirrors. Pump routing optics: (P1), (P8), (P12) polarization rotators; (P2), (P13) thin-film polarizers; (P9), (P14) lenses; (P9), (P15), (P16) HR flat mirrors. Laser routing optics: (17), (21) HR flat mirrors; (18) periscope; (19), (20) mirror telescope.

Pumping beams are focused into the crystal from opposite sides by lenses (P10), (P14). After amplification, the pulse is compressed to ~50 fs in double-pass two-grating compressor. After compressor it contains ~ 8 mJ energy at ~744-nm wavelength. Next, the radiation is frequency tripled (λ=0.248 nm) in two successive non-linear processes – by means of second harmonic generation (λ=0.372 nm) in 150-μm-thick BBO (type I) crystal and collinear mixing of the fundamental and 2ω beams in another 100-μm-thick BBO (type I) crystal. The efficiency of 2 ω and 3ω conversion is >30% and 4-8%, respectively. The output laser beam is linearly-polarized and has diameter of 8 mm. The Ti:Sapphire system operates with 0.5 mJ at λ=248 nm and repetition rate up to 10 Hz or in single shots synchronized with GARPUN laser system.

The spectra of master oscillator and 3ω output radiation were measured by spectrometers. Typical spectra are shown in Fig. 12. Pulse durations at λ=744 and 248 nm measured by an autocorrelator were ≤50 fs and ≤60 fs, respectively. To conclude, the parameters of Ti:Sapphire front-end are presented in Table 1.

To date, Ti: sapphire front-end has been synchronized with KrF master oscillator of GARPUN laser facility. Figure 13 demonstrates combined short (~60 fs) and long (~20 ns) pulses measured with Torlabs high-speed silicon photodiode DET 210 M with 1-ns time resolution. As they were registered by a 200 MHz, 2 GS/s TDS 2024 Tektronix oscilloscope, the short pulse looks broadened. Short and long pulses can be gradually moved one with respect to the other.

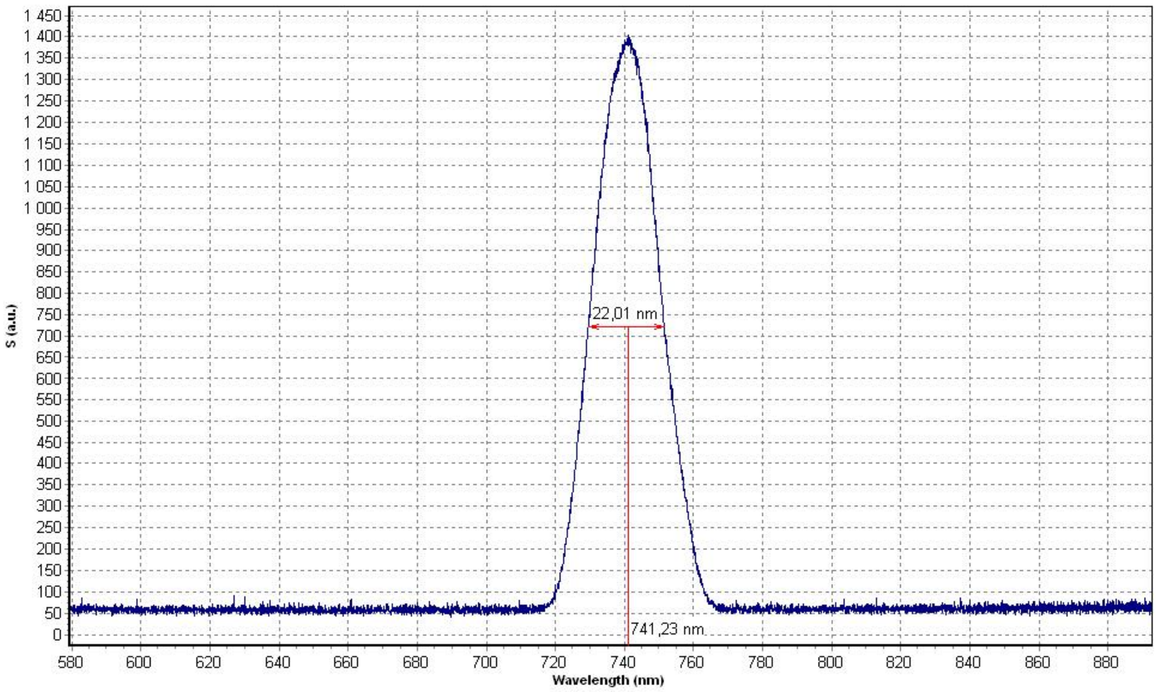

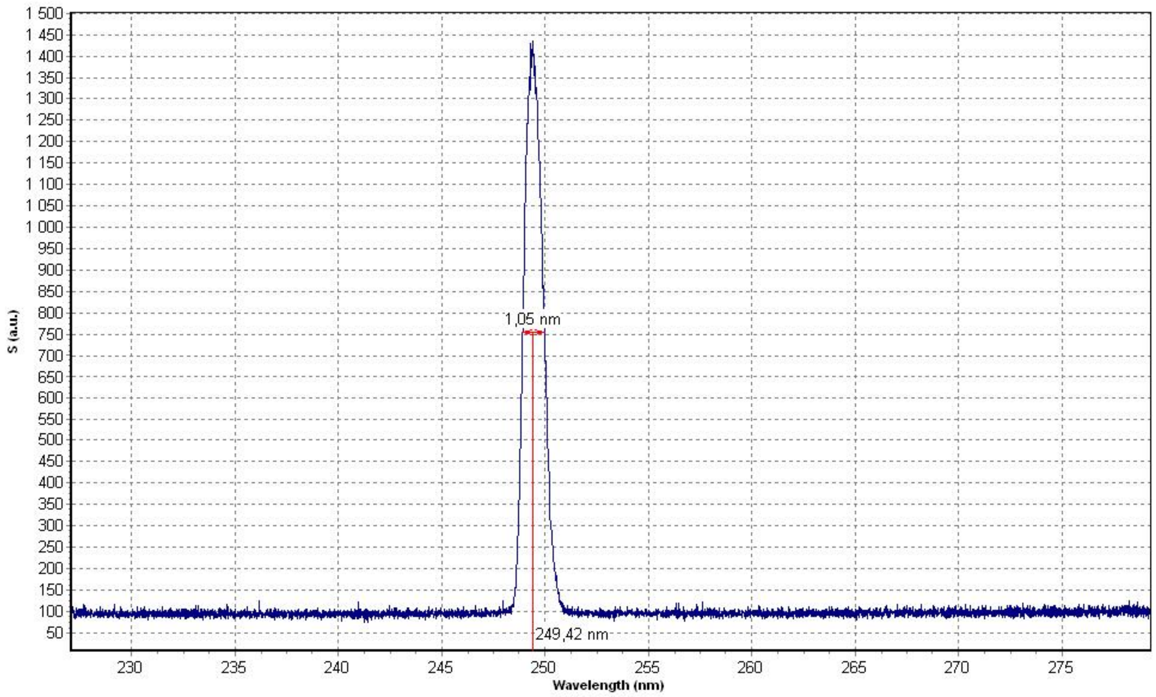

Fig. 12. The spectra of TiS-20 master oscillator (upper) and output radiation (bottom).

Pilot experiments on amplification of a short pulse in double-pass configuration in the discharge-pumped amplifier were performed and a gain factor of 5 was measured with output energy of ~1.5 mJ. This corresponds to energy density of 6.5 J/cm^2, which is 3.25 times more than saturation density Q_s.

Table 1. Parameters of Ti:Sapphire "START-248 M" laser system

Repetition rate	0-10 Hz
Pulse width at λ=744 nm	< 50 fs
Pulse width at λ=248 nm	< 60 fs
Pulse energy (@ 10 Hz) at λ=744 nm	> 8 mJ
Pulse energy (@ 10 Hz) at λ=248 nm > 0.5 mJ	> 0.5 mJ
Beam diameter at λ=744 nm	10 mm
Beam diameter at λ=248 nm	8 mm
Stability of energy at λ=744 nm	< 3%
Stability of energy at λ=248 nm	< 5%

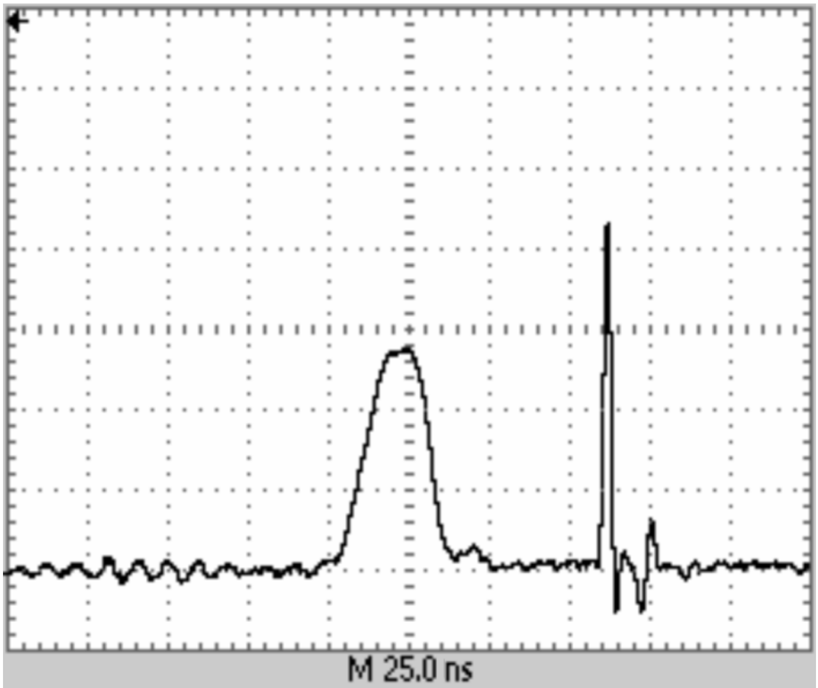

Fig. 13. Synchronized laser pulses of KrF master oscillator (left) and Ti:Sapphire front-end (right).

5. Gain and absorption measurements in GARPUN amplifier

Before short pulses are amplified in e-beam-pumped amplifiers, an extraction efficiency as well as gain and absorption properties of these devices have been determined for nanosecond pulses (Zvorykin *et al.*, 2005, 2006 a). The layout of experiments is shown schematically in Fig. 14.

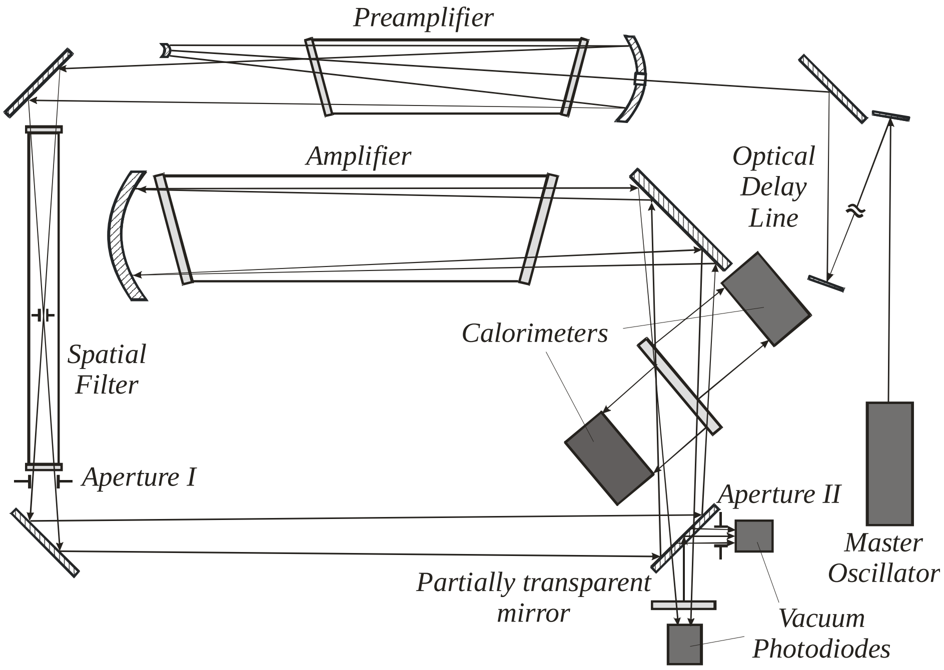

Fig. 14. Layout of amplification experiments.

A pulse of KrF master oscillator after passing an optical delay line was amplified in three passes in BERDYSH preamplifier and then transmitted through a spatial filter (a vacuum tube of 6-m length with variable aperture in a focal plane) to reduce the ASE of the preamplifier. Aperture I was set after the filter to select the most uniform part of the beam. At the entrance of GARPUN amplifier, a slightly divergent laser beam had dimensions 5×7 cm and input energy ~ 0.5 J. A concave 8-m focal length mirror reflected it back at a small angle. Both input and output beams being almost fully overlapped in the amplifier were measured by means of calorimeters and vacuum photodiodes.

Typical waveforms of laser pulses are shown in Fig. 15, where oscilloscope traces combines input (first) and output (second) pulses before and after final amplifier. The traces illustrate the pulse of master oscillator passing through preamplifier and amplifier without pumping (a), amplification in the preamplifier with switched-off amplifier (b), and the result of complete double-pass amplification (c, d). For larger aperture in a spatial filter (c), the ASE of preamplifier was not completely eliminated and it is seen as a precursor to the pulse amplified in final amplifier. Broadening of the master oscillator pulse in the preamplifier from initial 22 ns to 30 ns FWHM was caused by its high amplification length of ~3.4 m. It resulted in the saturation of the peak and relative growth of the low-intensity tail of the pulse. During the first pass in the amplifier, a front end of the input pulse was amplified alone in the active medium depleted only by the ASE. For a distance of ~2 m between front boundary of the gain region and the back mirror, reflected radiation completely overlapped with the rest part of the "incident" pulse within ~12 ns which resulted in its less amplification.

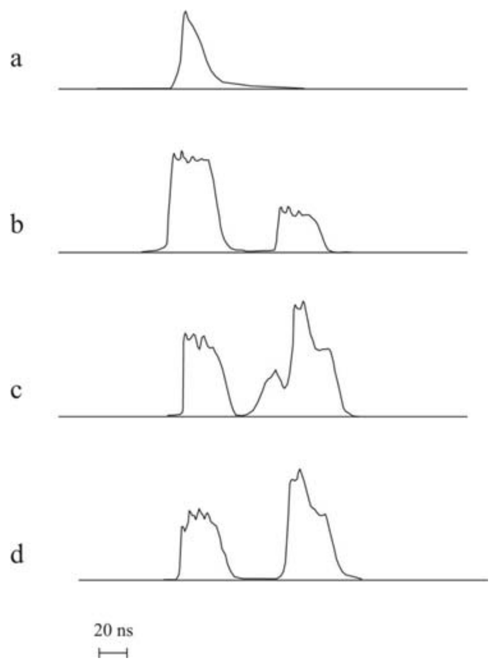

Fig. 15. Waveforms of master oscillator pulse (a), input and output pulses (not in scale) with switched-on preamplifier and without (b) or with (c, d) amplifier; (c) demonstrates high level of ASE with larger aperture in the spatial filter.

To account for losses of laser beam at several turning mirrors of the optical path and at uncoated optical windows of the amplifier, a ratio T_0 of output to input signals was measured with argon-filled laser chamber without e-beam pumping. To determine absorption in molecular fluorine, similar ratio T_f was measured with a working gas filling the chamber. The absorption coefficient for two passes is $\alpha_f = \frac{1}{2L_0}\ln\frac{T_0}{T_f}$, where L_0=140 cm is total length of the laser chamber. The measured values of α_f corresponded to absorption cross section of 1.2-1.5 $\times 10^{-20}$ cm^2 (Galvert & Pitts, 1966; Molchanov, 1988) and partial amount of fluorine in the mixture. Absorption in pure argon under e-beam pumping was measured in the same manner and absorption coefficient was determined: $\alpha_{Ar} = \frac{1}{2L}\ln\frac{T_{Ar}}{T_f}$, where L=100 cm is the length of pumped region.

Gain measurements were done for typical gas mixtures F_2/Kr/Ar = 0.2/6/93.8% at total pressures p=1.25 − 1.75 atm. Specific pumping power in the gain region of

GARPUN amplifier was determined earlier from the total e-beam energy deposition measured by means of a magnetically-inductive pressure gauge and from pumping distribution monitored by ArO fluorescence (Arlantsev *et al.*, 1994). It was in the range W_b= 0.65 − 0.8 MW/cm^3. The total stage gain $G = I_{out} / I_{in}$ is

$$G = \frac{T}{T_0^{L/L_0} T_f^{1-L/L_0}}, \quad (1)$$

where I_{in} and I_{out} are intensities at the entrance and exit of the gain medium, respectively; T are relevant ratios of input and output signals measured by calorimeters or photodiodes. This formula accounts for all the losses along the optical path and absorption in the "dead" unpumped regions inside the laser chamber nearby optical windows. For input intensity I_{in} = 0.4 MW/cm^2, the averaged double-pass gain was measured to be G = 25 with an accuracy of 20%. This value for a given pumping rate of W_b=0.8 MW/cm^3 is somewhat higher than that obtained by numerically simulating (see below Figs. 17 and 18). Thus, the intrinsic efficiency $\eta = \frac{I_{out} - I_{in}}{W_b L}$ =12%, although error of these measurements was rather high.

The results of gain measurements for a single-pass amplification scheme and wide range of input intensities are presented in Fig. 16. The experimental dependence $I_{out}(I_{in})$ is compared with numerical solutions of simple steady-state equation for radiation transfer along the amplifier axis z:

$$\frac{dI}{dz} = \left(\frac{g_0 - \alpha_s}{1 + I / I_s} - \alpha_{ns} \right) I \,. \quad (2)$$

Two parameters $g_0^{net} = g_0 - \alpha_s - \alpha_{ns}$ and I_s were varied to fit the solutions with the experimental data. The best agreement was achieved for the range of parameters g_0^{net} = (6.5−7.1) 10^{-2} cm^{-1} and I_s=1−2 MW/cm^2.

A small-signal gain coefficient $g_0 = g_0^{net} + \alpha_s + \alpha_{ns}$ can be then determined provided that saturable and nonsaturable absorption coefficients are known. Under our experimental conditions, at gas mixture pressure p=1.25 atm, we measured a part of nonsaturable absorption α_{Ar} due to short-lived exited species of argon, Ar^*, Ar_2^*, Ar_2^+: α_{Ar} = 5.3·10^{-3} cm^{-1}, as well as pump-independent absorption by F_2 molecules: α_f= 0.8·10^{-3} cm^{-1}. Then the lowest limit for nonsaturable absorption coefficient would be $\alpha_{ns} = \alpha_{Ar} + \alpha_f$ = 6.1·10^{-3} cm^{-1}. At higher gas mixture pressure p=1.75 atm, α_{Ar}= 8·10^{-3} cm^{-1}, α_f = 1.1·10^{-3} cm^{-1}, and α_{ns} = 9.1·10^{-3} cm^{-1}. These coefficients did not include other short-lived exited species in the gas mixture, such as F^-, Kr^*, Kr_2^*, Kr_2^+, $ArKr^*$, $ArKr^+$. As an amount of Kr in our gas mixtures was 15 times less than that of Ar, the measured values of α_{ns} seem to be reasonable.

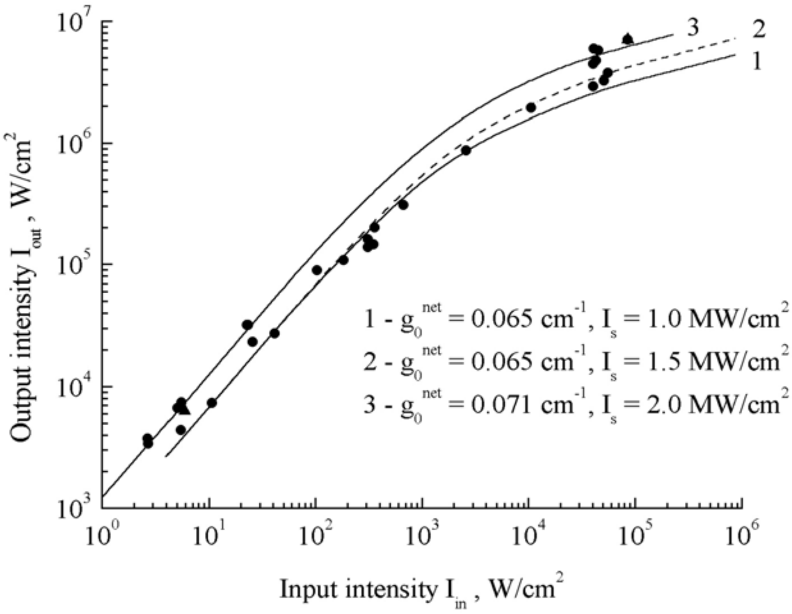

Fig. 16. Output intensity versus input intensity for single-pass amplification at gas pressure p= 1.25 (solid circles) and 1.75 atm (triangles); 1, 2, 3- various approximations with different amplification parameters.

Obtained g_0^{net} should be corrected taking into account depletion of the population inversion by ASE. A numerical quasi-stationary M-code was used for self-consistent calculations of the ASE and kinetic processes in large-aperture KrF lasers (Molchanov, 1988). Within generalized "forward – back" multi-direction approximation, a set of 6 simultaneous radiation transfer equations for so-called ASE waves and 2 equations for axial signal waves were solved together with kinetic equations for about one hundred reactions between several tens components involved into KrF active medium kinetics. Vibrational relaxation processes and temperature dependence of rate constants were included in the kinetics. A diffusive reflection of the ASE by sidewall of laser chamber was taken into account. For single-pass GARPUN amplifier at specific pumping power W_b=0.62 MW/cm^3, a small-signal gain coefficient was calculated to be $g_0 = 7.6 \cdot 10^{-2}$ cm^{-1}, nonsaturable absorption coefficient α_{ns}= $4.4 \cdot 10^{-3}$ cm^{-1}, saturable absorption coefficient $\alpha_s = 0.8 \cdot 10^{-3}$ cm^{-1}, and saturation intensity I_s = 1.53 MW/cm^2. Numerical simulation of I_{out} (I_{in}) dependence performed neglecting ASE demonstrated in the unsaturated region somewhat higher output intensities than in experiments. When the ASE was taken into account, I_{out} decreased 3−5 times. This gives for a depletion of the small-signal gain coefficient by the ASE $g_{ASE}/g_0 = (1+I_{ASE}/I_s)^{-1} = 0.79−0.84$ and average ASE intensity $I_{ASE} = 0.3−0.4$ MW/cm^2. By applying the same saturation factor to the experimental results, we obtain the corrected small-signal net gain coefficient $g_0^{net} = (7.7−9.0)\cdot 10^{-2}$ cm^{-1}. Note that numerical simulations with accounting for the ASE give 2-3 times less output intensities in the unsaturated region than experimental ones. As in this region $I_{out} \sim \exp(g_0 L)$ strongly depends on $g_0 L$ product, the discrepancy might be explained by minor theoretical error in g_0 or by underestimated e-beam pumping power and some enlargement of axial gain length due to electron scattering.

The simulations of double-pass GARPUN amplifier are shown in Figs. 17, 18 for an optimal gas mixture Ar/Kr/F_2 = 89.65/10/0.35% at the total pressure p = 1.4 atm and different specific pumping powers. As electron energy of about 300 keV was assumed be constant, variation in W_b corresponds to different current densities.

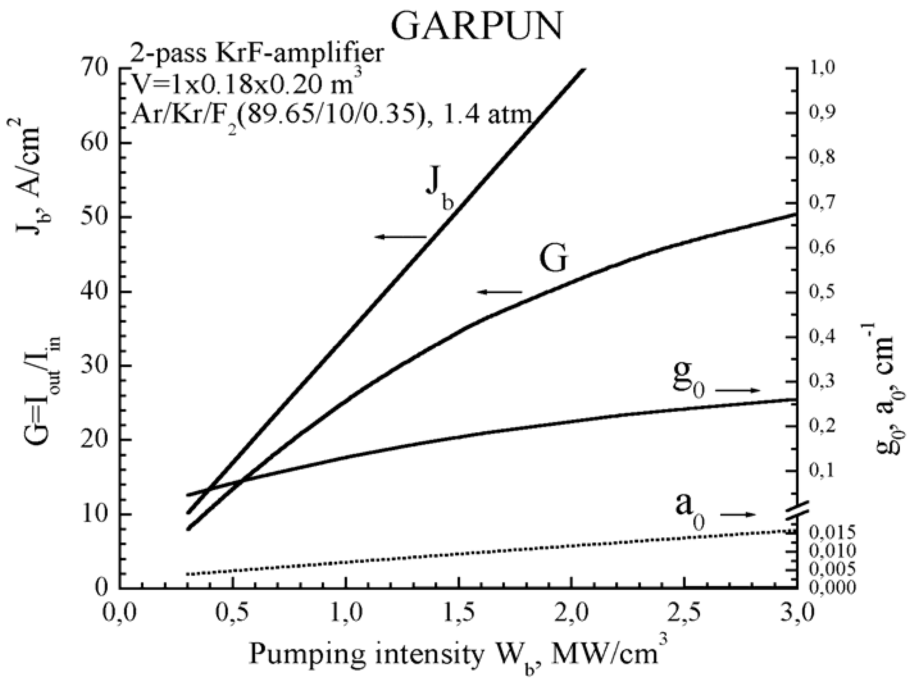

Fig. 17. Calculated small-signal gain and nonsaturable absorption coefficients, total gain $G=I_{out}/I_{in}$, e-beam current density J_b (for one of the two opposite beams) vs. specific pumping power.

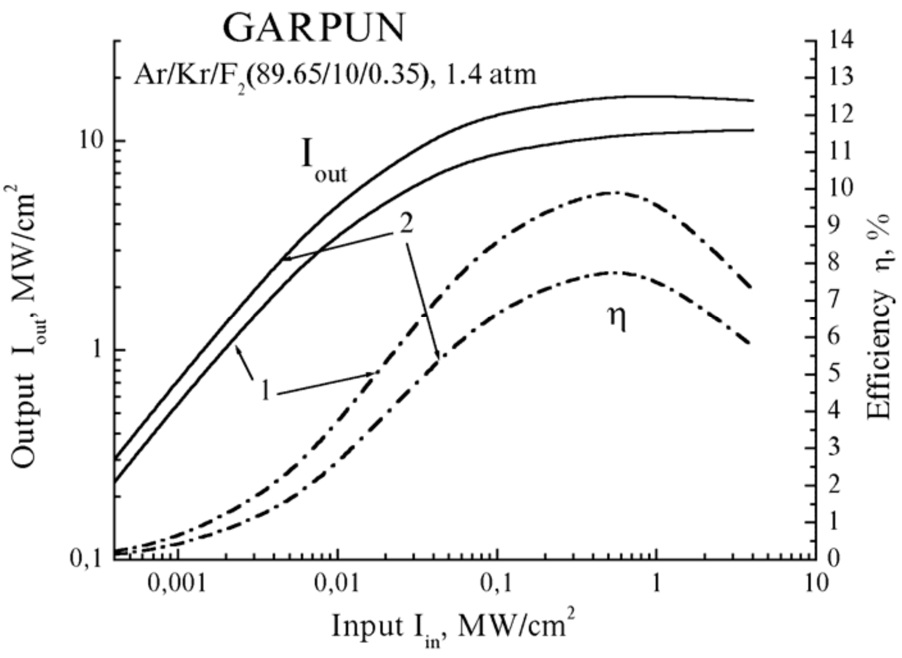

Fig. 18. Calculated output intensity and amplification efficiency vs. input intensity for double-pass GARPUN amplifier at different pumping intensities of 1 (1) and 2 MW/cm^3 (2).

6 Amplified spontaneous emission in GARPUN amplifier

In large-aperture KrF amplifiers and oscillators, ASE can considerably reduce the output laser energy. In a short-pulse laser-target interaction, ASE produces a pre-pulse at a target before arrival of the main UHI pulse, which is unacceptable in many applications. A ratio of the UHI pulse intensity (or energy density) at the target to corresponding values for the pre-pulse, which is referred to as a contrast ratio, is an important characteristic of laser system. In this section we discuss numerical simulations and experiments being performed at GARPUN amplifier to estimate expected ASE intensity on the target.

The same numerical M-code was used to calculate the ASE distribution in GARPUN amplifier in configurations of single-pass (without mirrors) and double-pass (with highly-reflecting back mirror) amplification schemes. All the ASE inside the laser chamber was represented by six ASE waves with intensities being averaged over corresponding solid angles. They varied from initial values of Ω_1 = 3.0 10^{-2} sr (in longitudinal direction) and Ω_2 = 1.7 sr (transverse direction) up to 2π while the waves passed the pumped region. The examples of simulations are demonstrated in Fig. 19

for gas mixture $Ar/Kr/F_2$ = (89.65/10/0.35)% at p = 1.4 atm and specific pumping power W_b = 0.62 MW/cm^3.

a

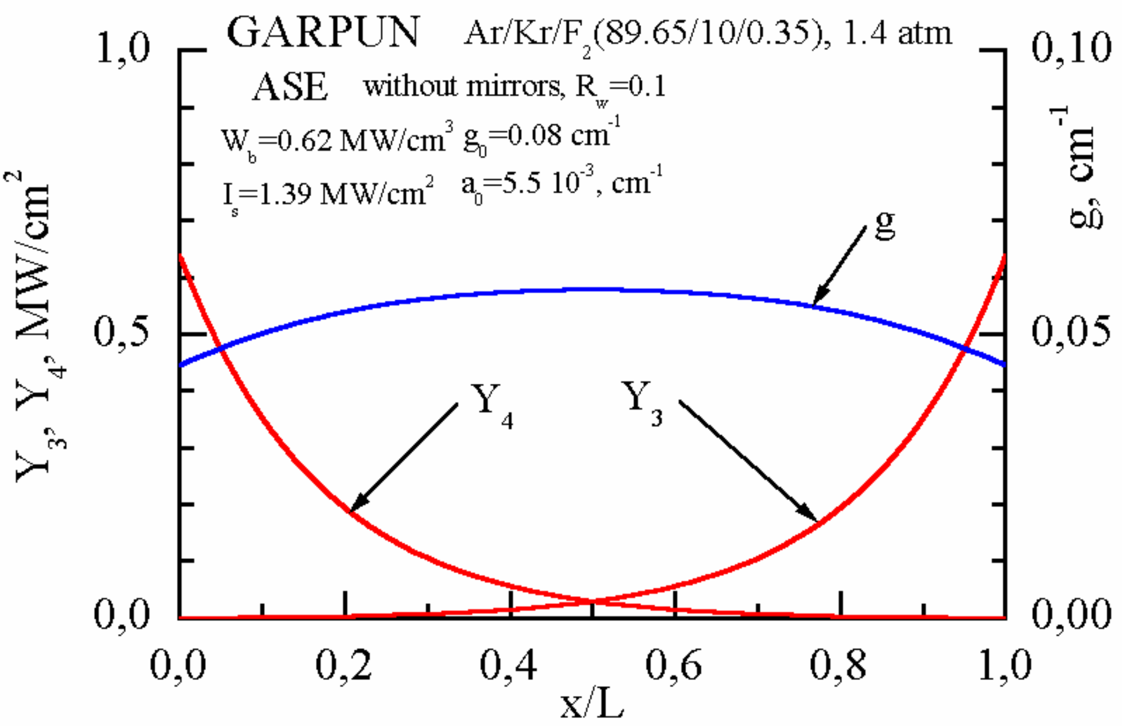

b

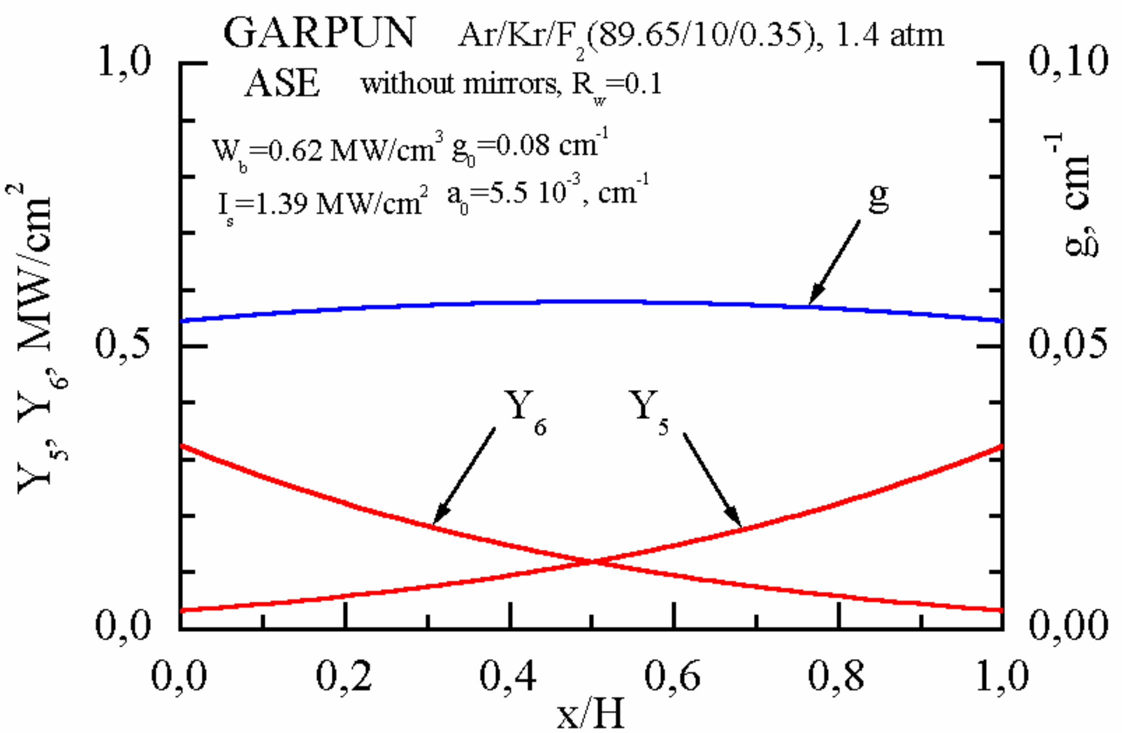

c

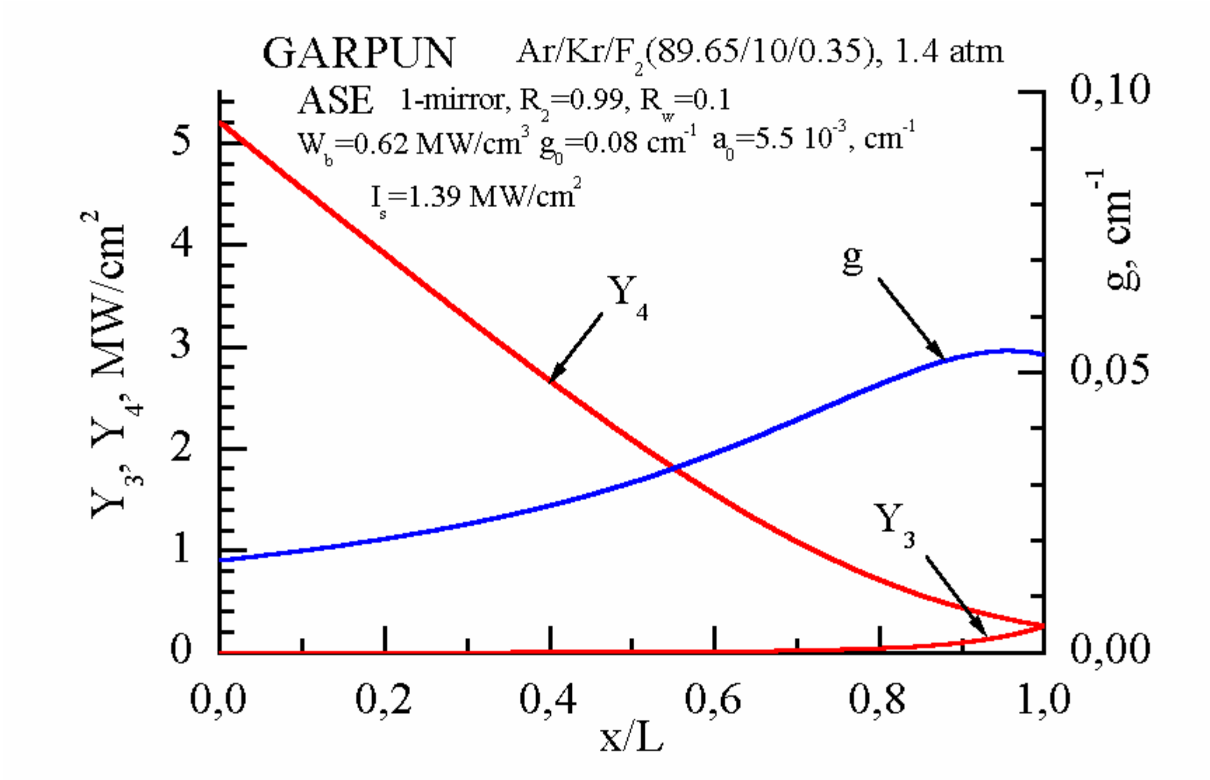

d

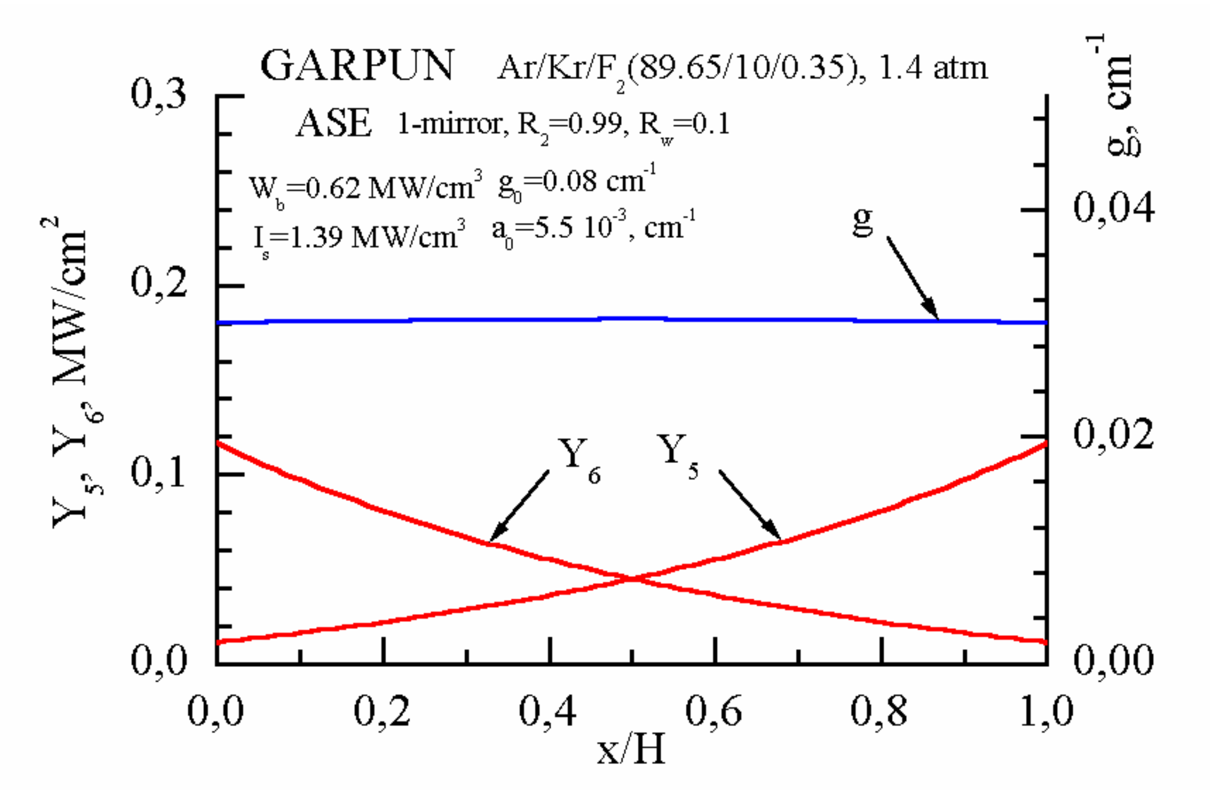

Fig. 19. Calculated distributions of ASE along the axis of GARPUN amplifier (a, c) and in transverse direction (b, d) in single-pass (a, b) and double-pass (c, d) schemes.

Layout of the experiments is shown in Fig. 20. The amplifier (1) operated under the same conditions as described above. In some laser shots, only one-half of pumping power was supplied by switching-off one of the two e-beams injected into the laser chamber from the opposite sides. In this case, of cause, the pumping power distribution across amplifier aperture became non-uniform; however, within the central region of amplifier close to its axis, the value of W_b was exactly one-half of the initial value. The axial ASE was measured in the "near field" in front of the amplifier window at the shortest available distance of 55 cm (designated by number 10 in Fig. 20), and in the "far field position" (8). In the former case, a sensitive calorimeter or vacuum photodiode (PD) measured the radiation that was emitted by the whole volume of excited gas in a wide range of solid angles. In the latter case, a large-aperture (300-mm-diameter) lens (4) was set close to the laser window and was combined with another one to focus the ASE from the whole gain volume on an iris aperture (10). It selected the radiation emitted in different small angles with respect to the amplifier axis. The iris diameter was varied from 3 to 30 mm that, for an effective focus of the lens system F_{eff} = 300 cm, corresponded to full divergent angles from 10^{-3} to 10^{-2} rad. To investigate the ASE in double-pass amplifier configuration, a back plane mirror (2) with reflectivity R_2 = 0.99 was set.

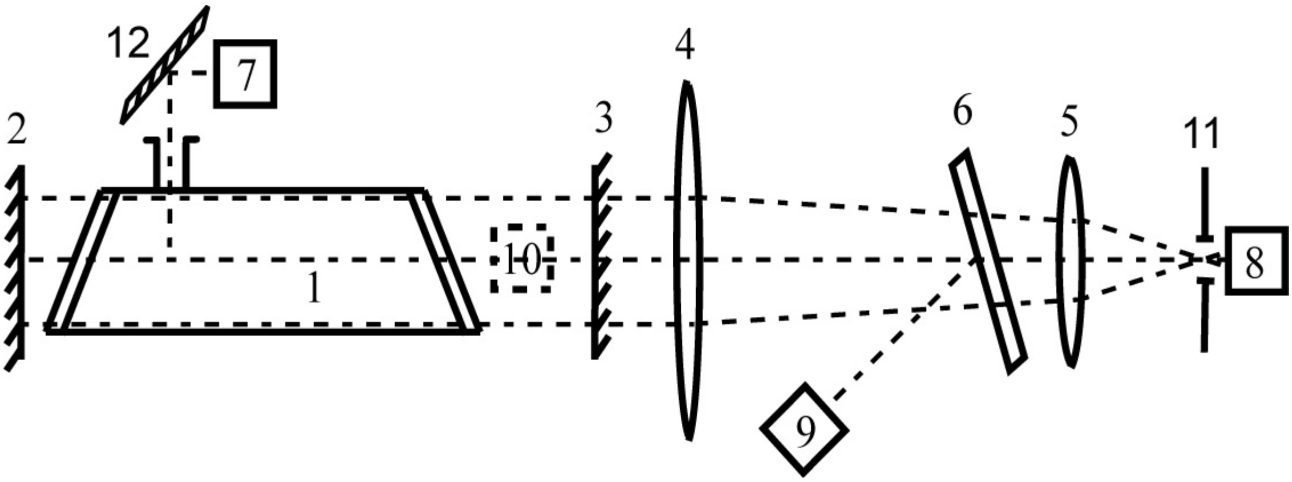

Fig. 20. Layout of the ASE measurements: (1) amplifier; (2), (3) back and front mirrors (optional); (4), (5) lenses; (6) plane SiO_2 plate; (7)–(10) calorimeters or photodiodes; (11) variable iris aperture; and (12) narrow-band reflecting mirror.

The results of near-field ASE measurements are presented in Table 2. The experimental data obtained in single-pass and double-pass schemes were recalculated to the front boundary of the pumped region to compare them with numerical simulations (see Fig. 19). For a single pass, this was done via multiplying by the factor $k_1 = \frac{1}{T}\left(\frac{L + l_d}{L}\right)^2$. First, by employing this factor, we take into consideration the total transmittance $T = T_w\ T_{F2}$ of the uncoated laser window (with $T_w = 0.92$) and unpumped 20-cm-long region inside laser chamber ($T_{F2} = 0.95$) adjacent to the window. Next, the second multiplier in the formula is a geometrical factor accounting for reduction in solid angle for the radiation detector set farther than the front boundary of pumped region. We assume that most of the ASE comes from the backside of pumped region of the length $L = 100$ cm; $l_d = 75$ cm is the distance from detector to the front boundary, thus $k_1 = 3.5$. For a double-pass scheme with a back mirror, the largest contribution is given by the radiation emitted near the front boundary and propagating through the amplifier twice. This radiation three times crosses the amplifier windows and unpumped regions. Hence, in this case, the correction factor is $k_2 = \frac{1}{T^3}\left(\frac{2L + l_d}{2L}\right)^2$. For real geometry of the experiment, one obtains $k_2 = 2.83$.

Table 2. Comparison of near-field ASE measurements with numerical simulations.

Experimental conditions: pumping & amplification configuration	Measured values		Recalculated values		Simulated values
	Energy density, mJ/cm^2	Intensity, MW/cm^2	Energy density, mJ/cm^2	Intensity, MW/cm^2	Intensity, MW/cm^2
Full pumping & single-pass	6.5	0.16	22.8	0.56	0.63
Full pumping & double-pass	66.4	1.64	188	4.64	5.2
Half pumping & single-pass	2.0	0.05	7.0	0.18	-
Half pumping & double-pass	3.5	0.086	9.9	0.24	-

The ASE pulse waveforms for both measurements were nearly identical with FWHM duration $\tau_{1/2}$ = 40 ns (Fig. 21). It was significantly shorter than the duration of pumping pulse (~100 ns). Seemingly, this "sharpening" of the axial ASE waveform was caused by an exponential factor with the index of exponent being proportional to instantaneous value of pumping power.

It is seen from Table 2 that recalculated values of the peak ASE intensity are in a good agreement with simulated ones for the specific pumping power W_b = 0.62·MW/cm^3 (Fig. 19). The measured ratio of the ASE signal in the double-pass measurements to that in the single-pass ones is 8.25, which coincides with simulated data. Note that for a half pumping scheme, this ratio falls down to 1.72 because of lower amplification exponent.

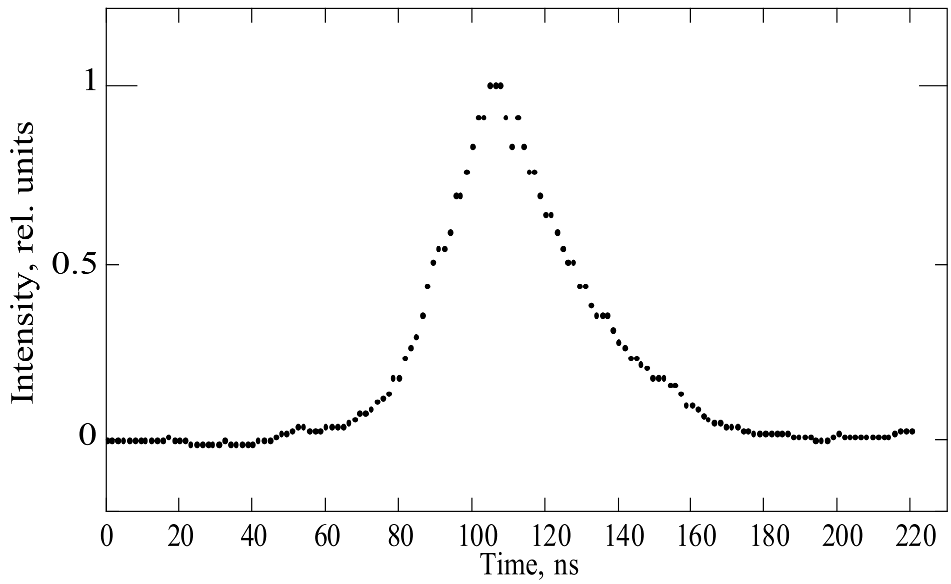

Fig. 21. Pulse waveform of the ASE along the amplifier axis measured by PD.

Far-field zone ASE was measured in a single-pass configuration to be proportional to the solid angle (Fig. 22). The pulse waveform had the same duration $\tau_{1/2}$ = 40 ns as was registered near the amplifier window. These gave for the ASE power per solid angle, $\frac{dW_{ASE}}{d\Omega}$ = 3.5·10^9 W/sr. Then ASE intensity at any distance r from the back boundary of the pumped region in amplifier can be expressed as $I_{ASE} = \frac{1}{r^2}\frac{dW_{ASE}}{d\Omega}$. The dependence of the ASE on the output aperture was measured by setting different masks on the amplifier window. It appeared that ASE energy was proportional to the open area confirming a good uniformity of GARPUN amplifier gain profile in the transverse direction. To investigate the dependence of the ASE on specific pumping power, one of the two oppositely-directed e-beams was switched off, while only a 50-mm-diameter opening remained on the central part of the amplifier aperture. In this case, for halved W_b = 0.31 MW/cm^2, the ASE reduced by 13 times. Note that in the case of completely opened amplifier aperture, this ratio was lower being equal to 3.25 (see Table 2).

For the ASE intensity on a target, similar relation $I_{ASE}^{t\arg} = \frac{1}{F^2}\frac{dW_{ASE}}{d\Omega}$ can be written where F is a focal length of focusing optics. If, for instance, F = 30 cm in a single-pass amplifier configuration under usual pumping conditions, $I_{ASE}^{t\arg}$ = 4 MW/cm^2. For a double-pass GARPUN configuration this value would be 8.25 times more. Note that for long enough amplification length, when the ASE intensity inside amplifier $I_{ASE} \geq I_s$, I_{ASE} begins to grow linearly with the length (see Fig. 19). At still longer lengths, the ASE intensity tends to saturate at the level $I_{ASE} = (g_0 /\alpha_{ns})I_s \approx 20$ MW/cm^2, which is 4 times more than the output value for double-pass GARPUN amplifier. In the limit, the ASE intensity on a target for a successive double-pass amplification of short pulses in both BERDYSH and GARPUN amplifiers will be about 100 MW/cm^2, which is near the threshold for plasma formation by 100-ns irradiation pulse (Bakaev *et al.*, 2005).

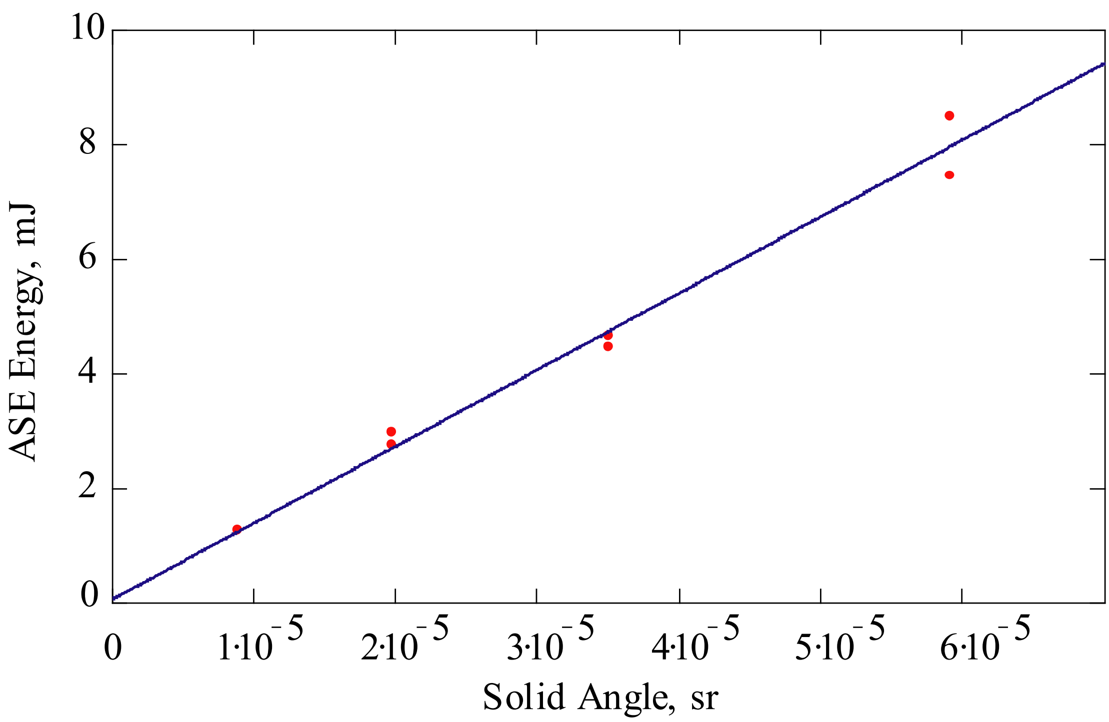

Fig. 22. The ASE energy in a far-field zone vs. solid angle for single-pass configuration.

7. Fluorescence and transient absorption spectra of $Ar/Kr/F_2$ mixtures

Emission spectra of $Ar/Kr/F_2$ mixtures typical of KrF laser operation contain in the UV visible range besides KrF (B→X) laser transition band at 248-nm wavelength other emission bands associated with C→A transition of KrF molecule with a maximum around 275 nm and a broad band of $4^2\Gamma \rightarrow 1{,}2\ ^2\Gamma$ transition of Kr_2F triatomic molecule centered at 405 nm (see, e.g., McDaniel & Nighan, 1982; Huestis *et al.*, 1983, and references therein). As they were measured earlier in arbitrary units, it is impossible to deduct relative intensities for different bands, which is of our peculiar interest for comparison with our quasi-stationary numerical M-code. This will allow us more accurate accounting for some important kinetic reactions. In particular, the formation of Kr_2F molecules, which, first, characterizes one of the main quenching processes of the upper KrF laser level in three-body collisions with Kr and Ar atoms (Kimura & Salesky, 1986), and, second, is an absorber of KrF laser radiation that might significantly affect the extraction efficiency of laser radiation from the gain medium. It should be noted that the absorption spectra were mostly obtained under conditions quite different from e-beam-pumped KrF laser and sometimes are contradictory in regard of the shape of absorption bands. Additional reason for the research of time-resolved spectra of spontaneous emission together with transient absorption spectra is feasibility to use some broad emission bands of diatomic and triatomic molecules for simultaneous amplification of short laser pulses at other wavelengths in the gain medium of KrF laser (Molchanov, 2006). Laser oscillations at trimer Kr_2F ($4^2\Gamma \rightarrow 1{,}2\ ^2\Gamma$) transition were obtained in the afterglow of e-beam pumping at very high specific input power of several tens of MW/cm^3 and high working gas pressures up to 8.5 atm (Tittel *et al.*, 1980). Lasing occurred within a broad band centered at ~430 nm. The gain volume and length were very small, ~ 0.04 cm^3 and 10 cm, respectively.

The layout of fluorescence and absorption measurements is shown in Fig. 23. Experiments were performed at BERDYSH amplifier module with a gas mixture $Ar/Kr/F_2$ = 91.8/8.9/0.3% at total pressure up to p = 1.8 atm. A black-body pulsed capillary-discharge light source "ISI-1", which has the brightness temperature T_b = 39±2 kK in the spectral range 220–600 nm (Demidov, *et al.*, 1970), was used for absorption measurements and relative calibration of wavelength response of the gauging equipment. A collimated probe beam was produced to pass along the laser axis. Then it was focused by a quartz condenser onto the entrance slit of a grating monochromator MDR-12. Transmitted radiation was registered by a photomultiplier (PM) together with a fluorescence signal (Fig. 24).

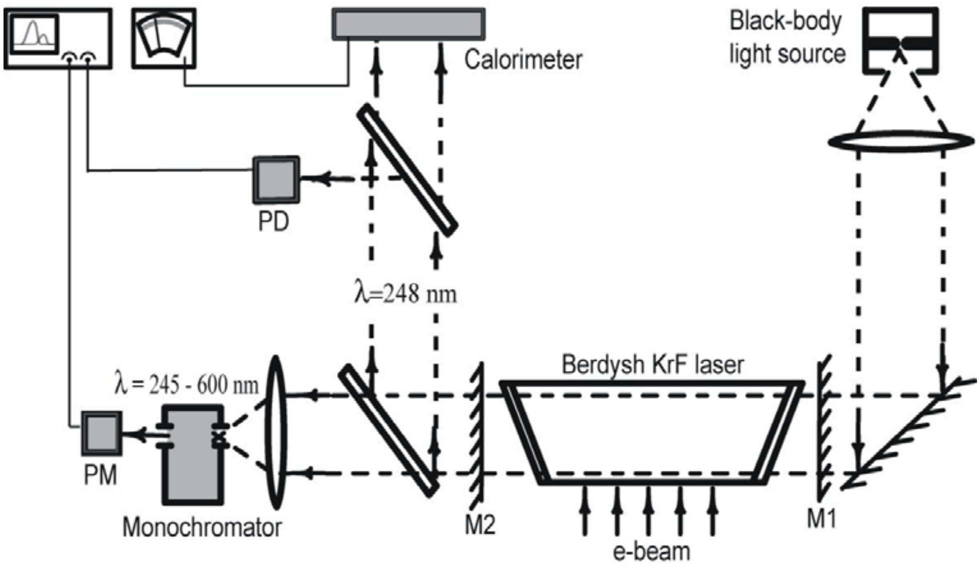

Fig. 23. Layout of fluorescence and absorption measurements.

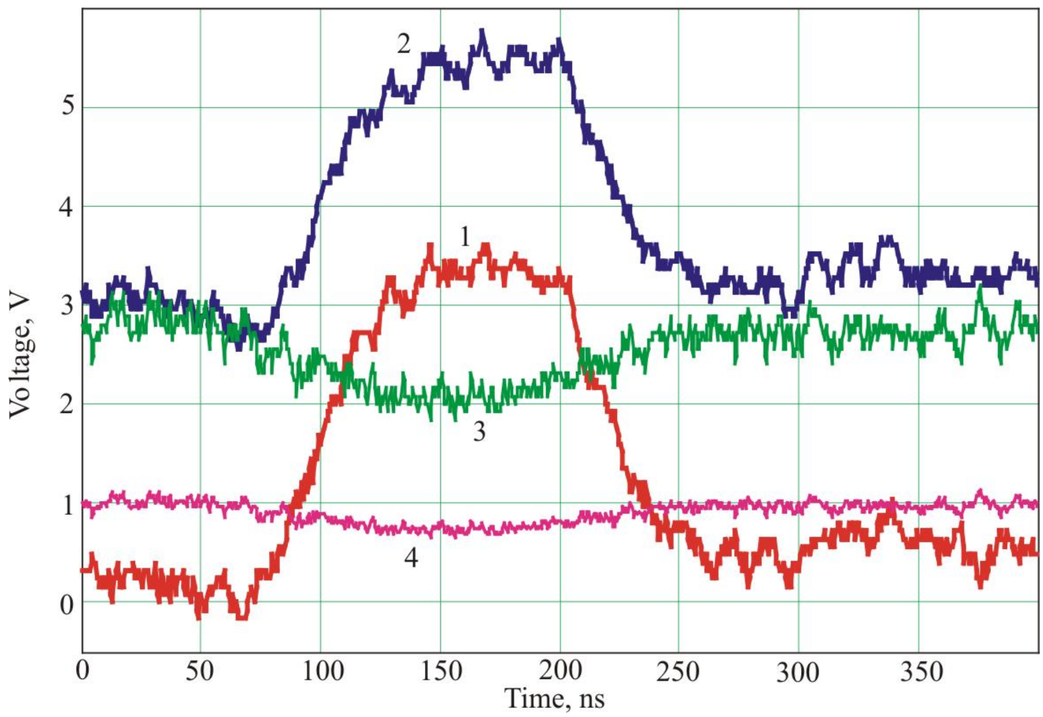

Fig. 24. Oscilloscope traces of gas fluorescence at 430-nm wavelength (1), its superimposition with the probe ISI-1 radiation (2), the difference signal (3), and normalized transient absorption (4).

Fluorescence spectra were plotted by amplitudes of fluorescence signals when probe radiation was blocked (Fig. 25). They represents the main emission bands KrF (B→X), KrF (C→A), and Kr_2F ($4^2\Gamma$→1,2 $^2\Gamma$) for two lengths of the gain medium of 110 and 7.5 cm. In the latter case, e-beam-pumped length was restricted by setting the mask. The spectra are in relative units and thus provide a comparison of the intensities of different emission bands. Significant growth of the maximum and narrowing of KrF (B→X) bandwidth is clearly seen in Fig. 25 for longer pumped length, which evidently demonstrates amplification of spontaneous emission at laser transition.

The lower state of triatomic molecule Kr_2F (1,2 $^2\Gamma$) is repulsive like that of KrF molecule, and one could expect population inversion and amplification at Kr_2F ($4^2\Gamma$→1,2 $^2\Gamma$) transition. By comparing spontaneous emission W_{KrF} and W_{Kr_2F} in KrF (B→X) and Kr_2F ($4^2\Gamma$→1,2 $^2\Gamma$) bands, we can estimate a small-signal gain coefficient. Integrating the spectra over corresponding bandwidths $\Delta\lambda_{KrF}$=2.5 nm and $\Delta\lambda_{Kr_2F}$=80 nm gives a value $\frac{W_{KrF}}{W_{Kr_2F}} = \frac{A_{KrF}\Delta\lambda_{KrF}}{A_{Kr_2F}\Delta\lambda_{Kr_2F}}\left(\frac{h\nu_{KrF}}{h\nu_{Kr_2F}}\right)$=17.8, where $\frac{A_{KrF}}{A_{Kr_2F}}$=350 is the ratio of maximums in wavelength distributions in Fig. 24. As $W_{KrF} = \frac{h\nu_{KrF}N^*_{KrF}}{\tau_{rKrF}}$ and $W_{Kr_2F} = \frac{h\nu_{Kr_2F}N^*_{Kr_2F}}{\tau_{rKr_2F}}$, where N^*_{KrF}, $N^*_{Kr_2F}$ are concentrations of the molecules in the upper states, τ_{rKrF}=6.5 ns and τ_{rKr_2F}=180 ns are corresponding radiative lifetimes (Quigley & Hughes, 1978; Geohegan & J.G. Eden, 1988), we obtain from the experiment $\frac{N^*_{KrF}}{N^*_{Kr_2F}}$=0.4. Note that quasi-stationary M-code for a working gas mixture under consideration and specific pumping power W_b = 0.64 MW/cm^2 gives N^*_{KrF} = $4\cdot10^{14}$ cm^{-3}, $N^*_{Kr_2F}$ = $8.76\cdot10^{14}$ cm^{-3}, and the calculated ratio $\frac{N^*_{KrF}}{N^*_{Kr_2F}}$=0.45 is close to the experimental one.

As a small-signal gain coefficient is given by expression $g_0 = \frac{\lambda^4 N^*}{4\pi^2c^2\Delta\lambda\tau_r}$, the ratio $\frac{g_{0KrF}}{g_{0Kr_2F}} = \frac{A_{KrF}}{A_{Kr_2F}}\left(\frac{\lambda_{KrF}}{\lambda_{Kr_2F}}\right)^4$=50. For a specific pumping power W_b=0.6-0.8 MW/cm^2 in present experiments, typical values of small-signal gain coefficient for KrF (B→X) are g_{0KrF} = 0.08–0.10 cm^{-1} (see Section 5). Therefore, for Kr_2F ($4^2\Gamma \rightarrow 1,2\ ^2\Gamma$) transition, one can estimate $g_{0Kr_2F} \approx 0.002$ cm^{-1}.

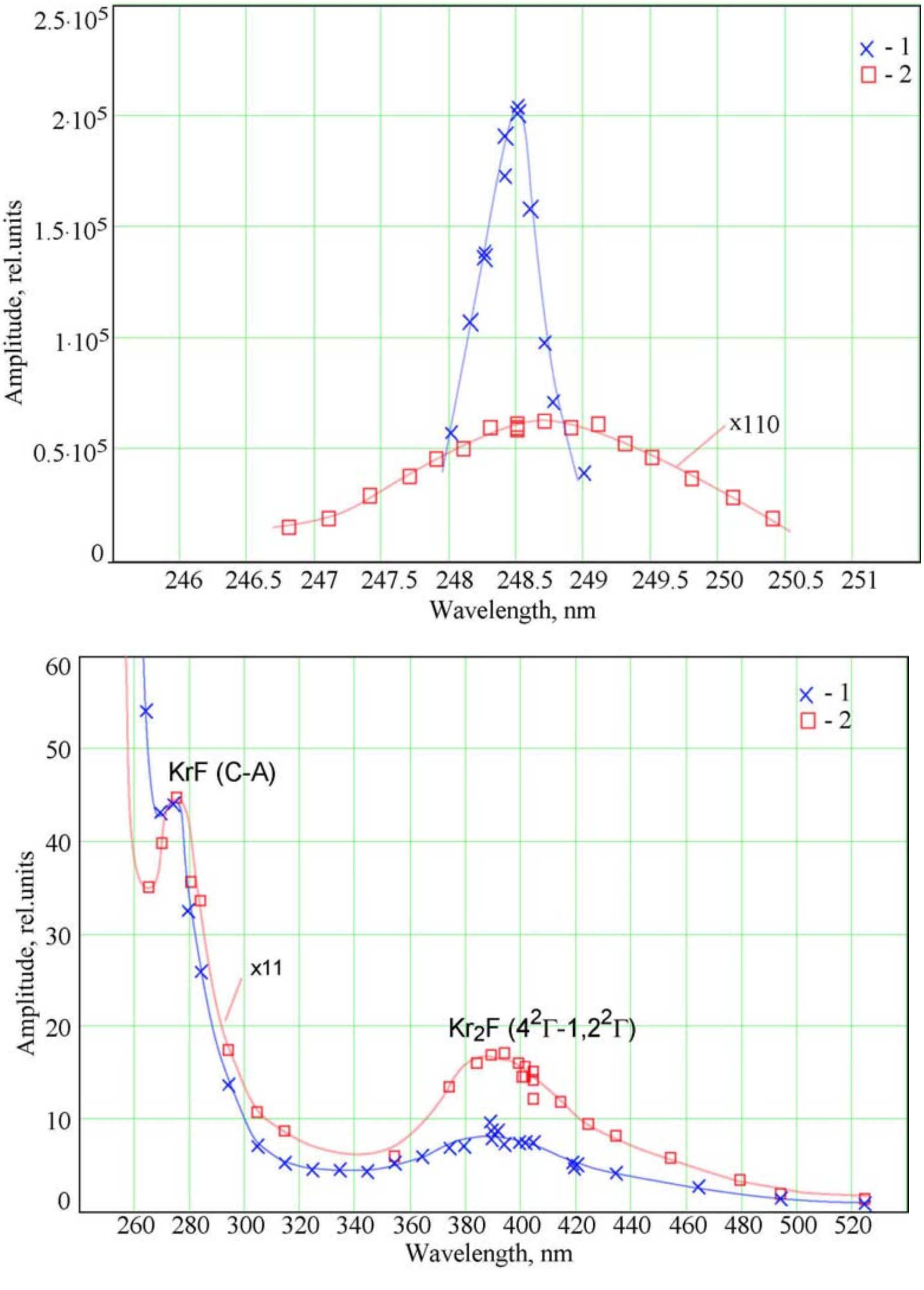

Fig. 25. Fluorescence spectra of Ar/Kr/F_2 = 91.8/8.9/0.3% gas mixture at p = 1.8 atm representing KrF (B→X) (upper), KrF (C→A) and Kr_2F ($4^2\Gamma \rightarrow 1,2\ ^2\Gamma$) transitions (bottom) for pumped lengths of L = 110 cm (1) and L = 7.5 cm (2). The values of (2) are multiplied by the factor of 110 (upper) and 11 (bottom).

As compared with the lower signal (1) in Fig. 24 when the fluorescence at 430-nm wavelength was the only registered by PM, the upper signal (2) is superimposed with the probe signal of the ISI-1. By deducting from the second signal the first one we obtain the difference signal (3), which reveals the reduction in amplitude due to transient absorption. By normalizing it to the initial value (before gas excitation), we have absorption A_λ (4) vs. time that enables us to derive an absorption coefficient $\alpha_\lambda = -\frac{1}{L}\ln A_\lambda(t)$ where L = 1.1 m is the length of pumped region. Note that the maximum of the absorption well coincides with the maximum of the fluorescence pulse.

The absorption spectrum for the peak absorption in the pulse was to-date recorded in limited wavelength range of 320-460 nm (Fig. 26). It is extended to shorter wavelengths in the UV region by the spectrum obtained by Schloss *et al*. (1997).

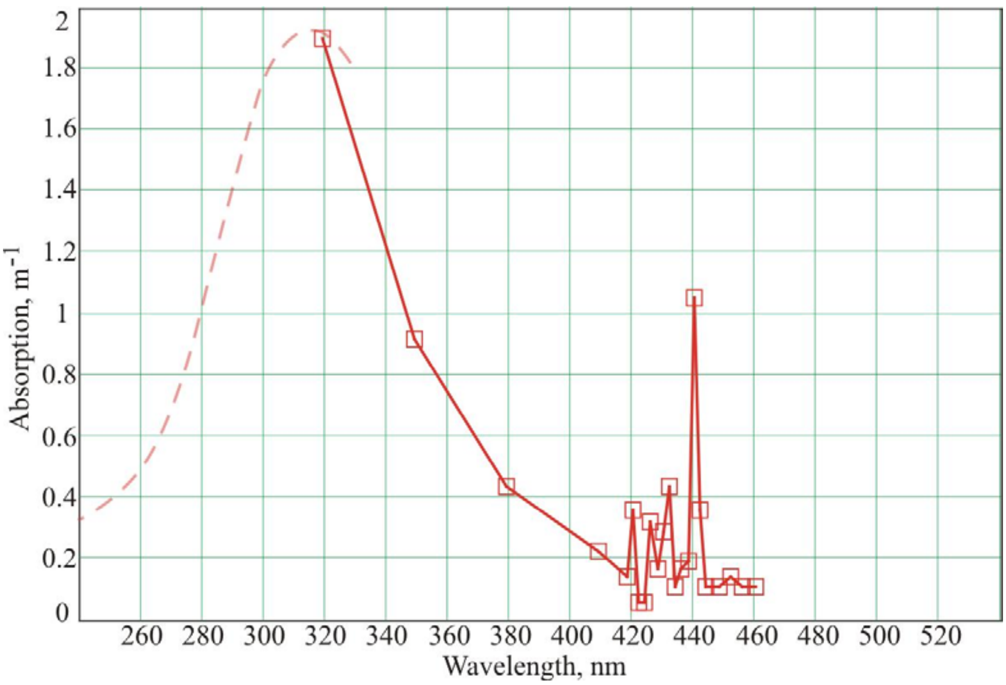

Fig. 26. Absorption spectra of Ar/Kr/F_2 = 91.8/8.9/0.3% gas mixture at p = 1.8 atm measured at the maximum of absorption pulse. Dashed line is a part of the spectra of Schloss *et al*. (1997).

A broad continuous absorption band, which begins from 420 nm and lasts to UV, originates due to photodissociation of Kr_2F ($4^2\Gamma$) molecule. The peak absorption during the pulse at 404-nm wavelength is α_λ ~ 0.2 m^{-1}. Therefore, there is a wide enough spectral range of about 400-440 nm where amplification of laser pulses at Kr_2F

($4^2\Gamma \rightarrow 1,2\ ^2\Gamma$) transition is expected to be slightly higher than absorption. Laser oscillations observed earlier at this transition by Tittel *et al.*, (1980) were centered near the wavelength of 435 nm where continuous absorption is less but amplification is strongly modulated by line absorption.

8. Numerical simulations of short pulse amplification

Non-coherent amplification of a short pulse successively in double-pass BERDYSH and GARPUN KrF-amplifiers was simulated using the equation (Kannari, 1990)

$$\frac{df}{dx} = g(x)\left(1 - e^{f}\right) - \alpha_{ns}(x) f\ , \qquad 0<x<L, \tag{3}$$

where $f = Q/Q_s$, $g\ (x) = \sigma N^*_{KrF}(x)$, $Q = \int I(x,t')dt'$.

To reduce ASE in the amplifiers, it was assumed that a long pulse with duration equal to the pumping time ($\tau_{long} = \tau_p$ =100 ns) and intensity $I_{in} = 10^{-3} I_s$ was supplied to the entrance of the amplifiers chain. This quasi-steady radiation together with the ASE forms longitudinal profiles of gain $g(x)$ and absorption $\alpha_{ns}(x)$ coefficients, which are used afterwards in Eq. (3). The energy of a short pulse at the entrance of the first BERDYSH amplifier was assumed to be E_{in} = 0.1 mJ, which corresponds to the energy of Ti:Sapphire front-end (see Section 4).

Figures 27, 28 demonstrate the dependences of the output energy density on the input energy density, both reduced to the saturation energy density Q_s, and distributions of Q/Q_s along the relative length of double-pass amplifiers. The output energies of 80 mJ and 1.6 J are expected for BERDYSH and GARPUN amplifiers, respectively. With the projected large-aperture DM amplifier, the energy in a single short pulse will increase up to 18 J while about 2 kJ is expected in long pulses.

9. Conclusions

Petawatt Excimer Laser Project (PEL Project) has started at P.N. Lebedev Physical Institute with the goal to generate ultra-high intensity subpicosecond pulses and to verify the fast-ignition ICF concept utilizing e-beam-pumped KrF drivers for simultaneous amplification of short & long laser pulses. At the present stage PEL Project implements up-grading of 100-J, 100-ns multi-stage GARPUN KrF laser facility by a femtosecond Ti:Sapphire front-end. Pilot experiments were performed to synchronize KrF and Ti:Sapphire master oscillators and to produce combined femtosecond/nanosecond pulses with variable time delay.

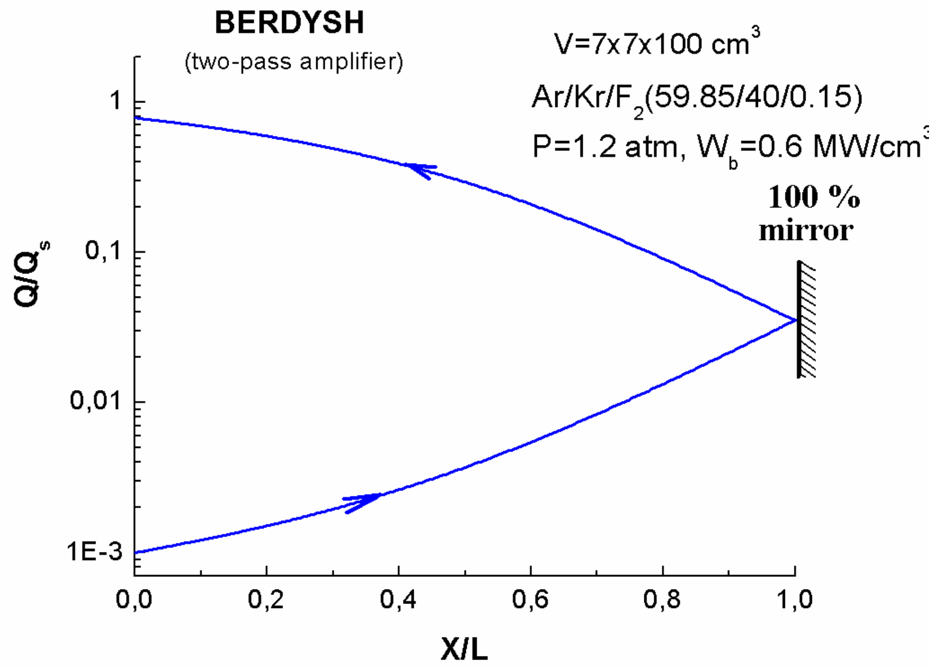

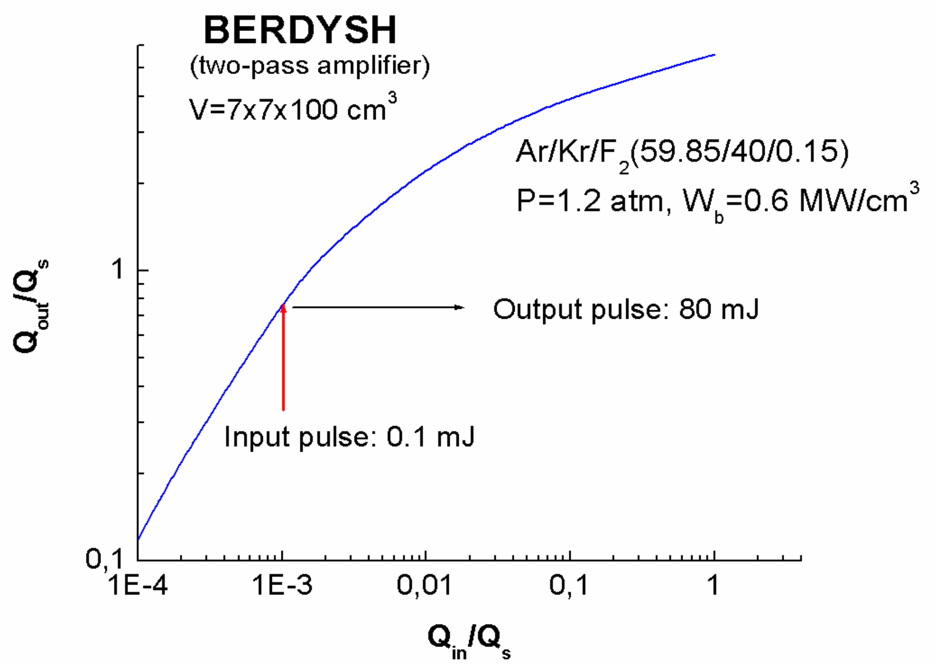

Fig. 27. Simulation of a short pulse amplification in double-pass BERDYSH amplifier: distribution of relative energy density along the relative length (top) and dependence of relative output energy density on the input one (bottom).

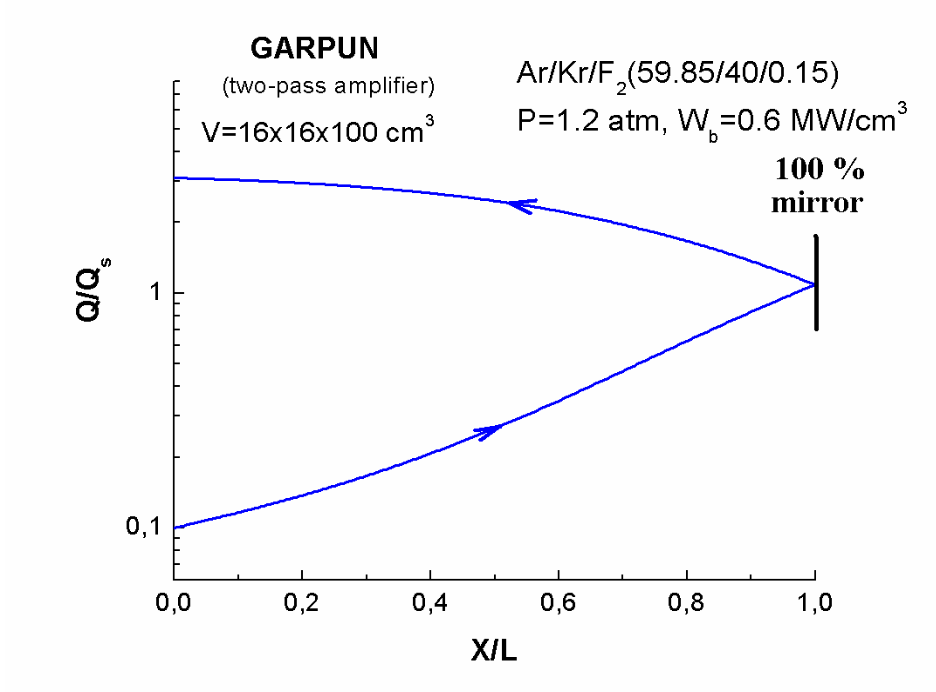

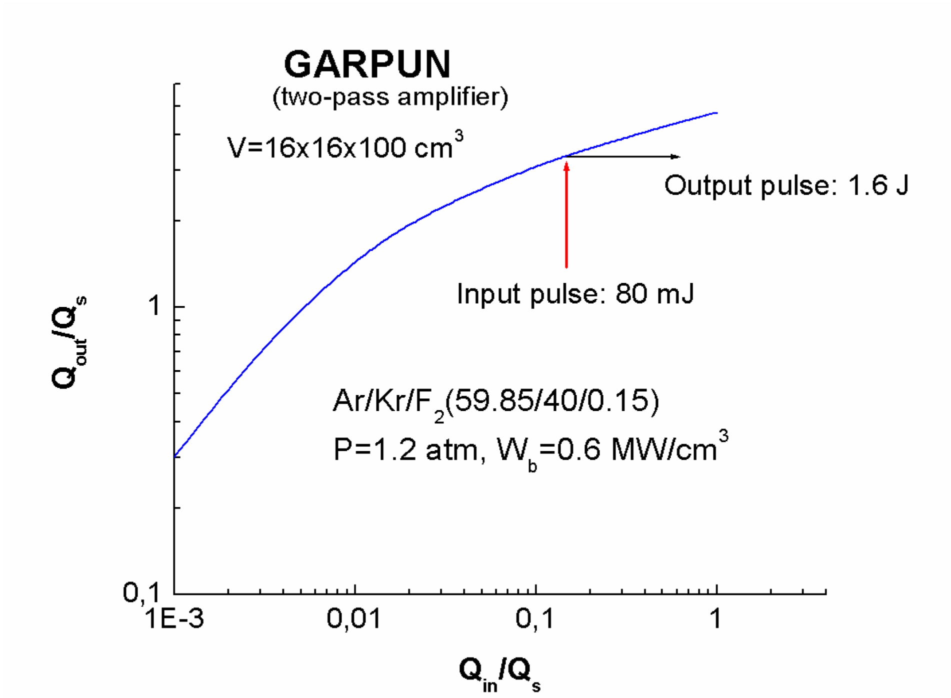

Fig. 28. Simulation of a short pulse amplification in GARPUN amplifier: distribution of relative energy density along the relative length (upper) and dependence of relative output energy density on the input one (bottom).

Gain and absorption measurements in GARPUN amplifier being compared with numerical simulations based on quasi-stationary numerical code precede future experiments on amplification of both short and combined pulses in e-beam-pumped large-aperture amplifiers. Amplified spontaneous emission was also measured and simulated to evaluate the pre-pulse intensity on a target produced by the amplifiers chain. To control the ASE level it was proposed to amplify short pulses in the medium depleted by quasi-steady laser radiation. Fluorescence and transient absorption spectra of $Ar/Kr/F_2$ mixtures conventionally used in KrF amplifiers were recorded to find out prospects for femtosecond pulse amplification at the broadband Kr_2F ($4^2\Gamma \rightarrow 1,2\ ^2\Gamma$) transition. Numerical simulations predict that 1.6 J can be obtained in subpicosecond pulse at multi-terawatt hybrid GARPUN-MTW Ti:Sapphire/KrF laser facility combined with several tens of joules in nanosecond pulse.

Acknowledgements

This research was implemented in the frame of the Programs of Russian Academy of Sciences "Fundamental problems of relativistic pulsed and stationary high-power electronics" and "Femtosecond optics and new optical materials". It was supported by Russian Ministry of Science and Education, Russian Fund for Basic Research (Project 05-02-16195), and also by US Naval Research Laboratory.

A.O. Levchenko and M.A. Rogulev were supported by Russian Academy of Sciences program for young scientists. A.O. Levchenko is also grateful to Russian Science Support Foundation.

REFERENCES

Aglitskiy, Y., Karasik, M., Serlin, V., *et al.* (2002). Direct observation of mass oscillations due to ablative Richtmyer-Meshkov instability and feedout in planar plastic targets. *Phys. Plasmas* **9**, 2264-2276.

Almasi, G., Szatmari, S., Simon, P. (1992). Optimized operation of short-pulse KrF amplifiers by off-axis amplification. *Opt. Commun.* **88**, 231-239.

Almasi, G., Szatmari, S. (1995). Optimization of multiple-pass off-axis KrF amplifiers. *Appl. Phys. B* **60**, 565-570.

Arlantsev, S.V., Grigor'yants, E.A., Vadkovskii, A.D., *et al.* (1994). Pumping of the GARPUN wide-aperture excimer laser by counterpropagating electron beams. *Quant. Electron.* **24**, 223-228.

Bakaev, V.G., Batani, D., Krasnyuk, I.A., *et al.* (2005) Hydrodynamics of high-energy GARPUN KrF laser interaction with solid and thin-film targets in ambient air. *J. Phys. D: Appl. Phys.* **38**, 2031-2044.

Basov, N.G., Bakaev, V.G., Bogdanovskii, A.V., *et al.* (1993). E-beam Pumped "Garpun" broadband KrF Laser with ~1GW Pulsed Lasing Power. *J. Sov. Laser Res.* **14**, 326-359.

Barr, J.R.M., Everall, N.J., Hooker, C.J., *et al.* (1988). High energy amplification of picosecond pulses at 248 nm. *Opt. Commun.* **66**, 127-132.

Bekesi, J., Szatmari, S., Simon, P., Marowsky, G. (2002). Table-top KrF amplifier delivering 270 fs output pulses with over 9 W average po.wer at 300 Hz. *Appl. Phys. B* **75**, 521-524.

Bibeau, C., Bayramian, A., Armstrong, P., *et al.* (2006). The mercury laser system – An average power, gas-cooled, Yb: S-FAP based system with frequency conversion and wavefront correction. *J. Phys. IV France*, **133**, 797-803.

Bigot, B. (2006). Inertial fusion science in Europe. *J. Phys. IV France*, **133**, 3-8.

Bouma, B., Luk, T.S., Boyer, K., Rhodes, C.K. (1993). High-brightness subpicosecond terawatt KrF* system driven with a frequency-converted self-mode-locked pulse-compressed Ti:Al_2O_3 laser. *J. Opt. Soc. Am. B* **10**, 1180-1184.

Bugaev, S.P., Abdullin, E.N., Zorin, V.B., *et al.* (2004). A 2-kJ wide-aperture XeCl laser. *Quantum Electronics* **34**, 801-804.

Demidov, M.I., Ogurtsova, N.N., Podmoshenskii, I.V. (1970). Pulsed black body with 40000^o and pulse duration 10^{-5} s. *J. Appl. Spectroscopy*, **12**, 365-367, (in Russian).

Divall, E.J., Edwards, C.B., Hirst, G.J., *et al.* (1996). Titania- a 10^{20} Wcm^{-2} ultraviolet laser. *J. Mod. Opt.* **43**, 1025-1033.

Ewing, J.J., Haas, R.A., Swingle J.C., *et al.* (1979). Optical Pulse Compression Systems for Laser Fusion. *IEEE J. Quantum Electron*., **QE-15**, 368-379.

Endoh, A., Watanabe, M., Sarukara, N., Watanabe, S. (1989). Multi-terawatt subpicosecond KrF laser. *Opt. Lett.* **14**, 353-355.

Freeman, R.R., Akli, K., Beg, F., *et al.* (2006). Overview of recent progress in US fast ignition research. *J. Phys. IV France*, **133**, 95-100.

Galvert, J.G. & Pitts, J.N. (1966). *Photochemistry*, New York: Wiley.

Geohegan, D.B., Eden, J.G. (1988). Absorption spectrum of $Kr_2F(4^2\Gamma)$ in the near ultraviolet and visible ($335 \leq \lambda \leq 600$ nm): Comparison with $Kr_2F^+(1(1/2)_u)$ measurements. *J. Chem. Phys*., **89**, 3410-3427.

Glownia, J.M., Misevich, J., Sorokin P.P. (1986). Ultrafast ultraviolet pump-probe apparatus. *J. Opt. Soc. Am. B* **3,** 1573-1580.

Harris, D.B., Allen, G.R., Berggren, R.R., *et al.* (1993). Strengths and weaknesses of KrF lasers for inertial confinement fusion applications learned from the AURORA laser. *Laser & Particle Beams*, **11**, 323-330.

Hernandez-Gomez, C., Brummitt, P.A., Canny, D.J., *et al.* (2006). Vulcan petawatt-operation and development. *J. Phys. IV France*, **133**, 555-559.

Hooker, C.J., Lister, J.M.D., Rodgers, P.A. (1991). Short pulse amplification in the ultraviolet stimulated Raman scattering. *Opt. Commun.* **82**, 497-502.

Houliston, J.R., Ross, I.N., Key, M.H., *et al.* (1994). Chirped pulse amplification in KrF lasers. *Opt. Commun.* **104**, 350-356.

Huestis, D.L., Marowsky, G., Tittel, F.K. (1983). In *Excimer Lasers* (Rhodes, C.K., Egger, H. and Pummer, H. Eds.) AIP, New York, pp. 181-215.

Hunter, A.M., Hunter, R.O., Johnson, T.H. (1986). Scaling of KrF lasers for inertial confinement fusion. *IEEE J. Quant. Electron.* **QE-22**, 386-404.

Kannari, F. (1990). Multilevel model analysis of energy extraction from a KrF laser medium by short pulse. *J. Appl. Phys.* **67**, 3954-3963.

Kawashima, T., Ikegawa, T., Kawanaka, J., *et al.* (2006). The HALNA project: Diode-pumped solid-state laser for inertial fusion energy. *J. Phys. IV France*, **133**, 615-620.

Kelly, J.H., Waxer, L.J., Bagnoud, V., *et al.* (2006). OMEGA EP: High-energy petawatt capability for the OMEGA laser facility. *J. Phys. IV France*, **133**, 75-80.

Key, M.H., Cable, M.D., Cowan, T.E., *et al.* (1998). Hot electron production and heating by hot electrons in fast ignitor research. *Phys. of Plasmas*. **5**, 1966-1972.

Kimura, W.D. & Salesky, E.T. (1986). Kr_2F^* fluorescence measurements of electron beam pumped KrF laser mixtures. *Appl. Phys. Lett.* **48**, 897-899.

Kodama, R., Shiraga, H., Shigemori, K., *et al.* (2002). Fast heating scalable to laser fusion ignition. *Nature*, **418**, 933-934.

Lowenthal, D.D., Ewing, J.J., Center, R.E., *et al.* (1981). Conceptual Design of an Angular Multiplexed 50 kJ KrF Amplifier for ICF. *IEEE J. Quant. Electron.* **QE-17**, 1861-1870.

McDaniel, E.W. & Nighan, W.L., Eds. (1982) *Applied Atomic Collision Physics*. Vol. **3**, *Gas Lasers*, Academic Press.

McGeoch, M.W., Corcoran, P.A., Altes, R.G., *et al.* (1997). Conceptual Design of a 2 MJ KrF Laser Facility. *Fusion Technology*, **32**, 610-643.

Lindl, J.D., Hammel, B.A., Logan G.B., *et al.* (2003). The US inertial confinement fusion (ICF) ignition programme and the inertial fusion energy (IFE) programme, *Plasma Phys. Control. Fusion* **45**, Suppl. 12A, A217-A234.

Luk, T.S., McPherson, A., Gibson, G., *et al.* (1989). Ultrahigh-intensity KrF* laser system. *Opt. Lett.* **14**, 1113-1115.

McIntyre, I.A. & Rhodes C.K. (1991). High power ultrafast excimer lasers. *J. Appl. Phys.* **69**, R1-R19.

Miyanaga, N., Azechi, H., Tanaka, K.A., *et al.* (2006). 10-kJ PW laser for the FIREX-I program. *J. Phys. IV France* **133**, 81-87.

Molchanov A.G. (1988). Theory of active media of excimer lasers. *Proc. of Lebedev Phys. Inst.* Vol. **171**, pp. 72-167. Nova Science Publishing, Commack.

Molchanov, A.G. (2006). Short pulse amplification in a KrF-laser and the petawatt excimer laser problem. *J. Phys. IV France* **133**, 665-668.

Moses, E.I., Miller, G.H., Kauffman, R.L. (2006). The ICF status and plans in the United States. *J. Phys. IV France* **133**, 9-16.

Murray, J.R., Goldhar, J., Eimerl, D., Szoke, A. (1979). Raman Pulse Compression of Excimer Lasers for Application to Laser Fusion. *IEEE J. Quant. Electron.* **QE-15**, 342-368.

Nabekawa, Y., Sajiki, K., Yoshitomi, D., *et al.* (1996). High-repetition-rate high-average-power 300-fs KrF / Ti: sapphire hybrid laser. *Optics Letters* **21**, 647-649.

Nabekawa, Y., Yashitomi, D., Sekikawa, T., Watanabe, S. (2001). 50-W average-power, 480-fs KrF excimer laser with gated gain amplification. *Optics Letters* **26**, 807-809.

Obenschain, S.P., Bodner, S.E., Colombant, D., *et al.* (1996). The Nike KrF laser facility: Performance and initial target experiments. *Phys. Plasmas*, **3**, 2098-2107.

Omenetto, F.G., Boyer, K., Longworth, J.W., *et al.* (1997). High-brightness terawatt KrF* (248 nm) system. *Appl. Phys. B* **64**, 643-646.

Owadano, Y., Okuda, I., Matsumoto, Y., *et al.* (1989). Development of a high-power KrF laser system, ASHURA. *Laser & Particle Beams,* **7**, 383-392.

Owadano, Y., Okuda, I., Matsumoto, Y., *et al.* (1993). Performance of the ASHURA KrF laser and its upgrading plan. *Laser & Particle Beams,* **11**, 347-351.

Owadano, Y., Okuda, I., Matsumoto, Y., *et al.* (1999). Overview of Super ASHURA KrF Laser Program. *Fusion Engineering and Design* **44**, 91-96.

Owadano, Y., Okuda, I., E., Matsushima, I., *et al.* (2001). KrF Laser Program at AIST. In *Inertial Fusion Sciences and Applications 2001*. (Tanaka, K.A., Meyerhofer, D.D., Meyer-ter-Vehn, J. Eds.), pp. 465-469. Elsevier.

Pawley, C.J., Gerber, K., Lehmberg, R.H., *et al.* (1997). Measurements of laser-imprinted perturbations and Rayleigh-Taylor growth with Nike KrF laser. *Phys. Plasmas,* **4**, 1969-1977.

Pawley, C.J., Sethian, J.D., Bodner, S.E., *et al.* (1999). Direct drive acceleration of planar targets with the Nike KrF laser. *Fusion Engineering and Design* **44**, 171-174.

Pessot, M., Maine, P., Mourou, G. (1987). 1000 times expansion/compression of optical pulses for chirped pulse amplification. *Opt. Commun.*, **62**, 419-421.

Quigley, G.P. & Hughes, W.M. (1978). Lifetime and quenching rate constants for Kr_2F^* and Kr_2^*. *Appl. Phys. Lett.*, **32**, 649-651.

Roberts, J.P., Taylor, A.J., Lee, P.H.Y., Gibson, R.B. (1988). High-irradiance 248-nm laser system. *Opt. Lett.* **13**, 734-736.

Ross, I.N., Damerell, A.R., Divall, E.J., *et al.* (1994). A 1 TW KrF laser using chirped pulse amplification. *Opt. Commun.* **109**, 288-293.

Rosocha, L.A., Bowling, P.S., Burrows, M.D., *et al.* (1986). An overview of Aurora: a multi-kilojoule KrF laser system for inertial confinement fusion. *Laser & Particle Beams*, **4**, 55-70.

Rosocha, L.A., Hanlon, J.A., McLeod, J., *et al.* (1987). Aurora Multikilojoule KrF laser system prototype for inertial confinement fusion. *Fusion Technology*, **11**, 497-531.

Sethian, J.D., Obenschain, S.P., Lehmberg, R.H., McGeoch, M.W. (1998). KrF Lasers for Inertial Fusion Energy. In *Proceedings of 17th IEEE/NPSS Symposium on Fusion Engineering, San Diego, CA, October 1997*, p. 593-597. Piscataway, NJ: IEEE.

Sethian, J.D., Obenschain, S.P., Lehmberg, R.H., McGeoch, M.W. (1999). A rep-rate KrF system to address the issues relevant to inertial fusion energy. *Fusion Engineering and Design*, **44**, 371-375.

Sethian, J.D. Friedman, M., Jiuliani Jr., J.L., *et al.* (2003). Electron beam pumped KrF lasers for Fusion Energy, *Phys. of Plasmas*, **10**, 2142-2146.

Scharzenbach, A.P., Luk, T.S., McIntyre, I.A., *et al.* (1986). Subpicosecond KrF* excimer-laser source. *Opt. Lett.* **11**, 499-501.

Shaw, M.J. (1991). Prospects for high-power KrF lasers. *Laser & Particle Beams,* **9**, 309-328.

Shaw, M.J., Bailly-Salins, R., Edwards, B., *et al.* (1993). Development of high-performance KrF and Raman laser facilities for inertial confinement fusion and other applications. *Laser & Particle Beams,* **11**, 331-346.

Shaw, M.J., Ross, I.N., Hooker, C.J., *et al.* (1999). Ultrahigh-brightness KrF laser system for fast ignition studies. *Fusion Engineering and Design* **44**, 209-214.

Sviatoslavsky, I.N., Sawan, M.E., Peterson, R.R., *et al.* (1992). A KrF Laser Driven Inertial Fusion Reactor “Sombrero”. *Fusion Technology* **21**, 1470-1474.

Szatmari, S., Schafer, F.P., Muller-Horsche, E.M., Muckenheim, W. (1987). Hybrid dye-excimer laser system for the generation of 80 fs, 900 GW pulses at 248 nm. *Opt. Commun.* **63**, 305-309.

Szatmari, S. & Schafer, F.P. (1988). Simplified laser system for the generation of 60 fs pulses at 248 nm. *Opt. Commun.* **68**, 196-202.

Szatmari, S. (1992). Terawatt-class hybrid dye / excimer lasers. In *Topics in Applied Physics*. (Stuke M. Ed.) Berlin: Springer. Vol. **70**, pp. 129-140.

Szatmari, S., Almasi, G., Feuerhake, M., Simon, P. (1996). Production of intensities of ~ 10^{19} W/cm^2 by a table-top KrF laser. *Appl. Phys. B* **63,** 463-466.

Szatmari, S. High-Brightness Ultraviolet Excimer Lasers. (1994). *Appl. Phys. B* **58**, 211-223.

Takahashi, E., Losev, L.L., Matsumoto, Y., *et al.* (2003). KrF laser picosecond pulse source by stimulated scattering processes. *Opt. Commun.* **215**, 163-167.

Takahashi, E., Losev, L.L., Matsumoto, Y., *et al.* (2005). 1 ps, 3 mJ KrF laser pulses generated using stimulated Raman scattering and fast Pockels cell. *Opt. Commun.* **247**, 149-152.

Taylor, A.J., Tallman, C.R., Roberts, J.P., *et al.* (1990). High-intensity subpicosecond XeCl laser system. *Opt. Lett.* **15**, 39-41.

Strickland, D. & Mourou, G. Compression of amplified chirped optical pulses. (1985). *Opt. Comms.* **56**, 219-221.

Tilleman, M.M., Jacob, J.H. (1987). Short pulse amplification in the presence of absorption. *Appl. Phys. Lett.* **50**, 121-123.

Tittel, F.K., Smayling, M., Wilson, W.L. (1980). Blue laser action by the rare-gas halide trimer Kr_2F, *Appl. Phys. Lett.* **37**, 862-864.

Von Rosenberg, C.W. Jr. (1992). KrF driver system architecture for a laser fusion power plant. *Fusion Technology,* **21**, 1600-1604.

Watanabe, S., Endoh, A., Watanabe, M., Sarukara, N. (1988). Terawatt XeCl discharge laser system. *Opt. Lett.* **13**, 580-582.

Watanabe, S., Endoh, A., Watanabe, M., *et al.* (1989). Multiterawatt excimer-laser system. *J. Opt. Soc. Am. B* **6,** 1870-1876.

Watanabe, M., Hata, K., Adachi, T., *et al.* (1990). High-repetition-rate terawatt excimer laser system with gated gain amplification. *Opt. Lett.* **15**, 845-847.

Wolford, M.F., Hegeler, F., Myers, M.C., *et al.* (2006). Efficient repetitively pulsed 730 joule electron beam pumped KrF laser. *J. Phys. IV France* **133**, 697-699.

Zvorykin, V.D., Lebo, I.G., Rozanov, V.B. (1997). On the feasibility of production of a source of thermonuclear neutrons on the basis of a KrF laser. *Bull. of Lebedev Phys. Inst.*, No. 9-10, 20-29.

Zvorykin, V.D. & Lebo, I.G. (1999). Laser and target experiments on KrF GARPUN laser installation at FIAN. *Laser & Particle Beams* **17**, 69-88.

Zvorykin, V.D., Arlantsev, S.V., Bakaev, V.G., *et al.* (2001). Transport of electron beams and stability of optical windows in high-power e-beam-pumped krypton fluoride lasers. *Laser & Particle Beams* **19**, 609-622.

Zvorykin, V.D., Bakaev, V.G., Lebo, I.G. Sychugov, G.V. (2004). Hydrodynamics of plasma and shock waves generated by high-power GARPUN KrF laser. *Laser & Particle Beams* **22**, 51-57.

Zvorykin, V.D., Bakaev, V.G., Levchenko, A.O., *et al.* (2005). Amplified spontaneous emission and nanosecond pulse amplification in large-aperture electron-beam-pumped KrF amplifiers, *Proceedings SPIE*, **5777**, 548-553.

Zvorykin, V.D., Arlantsev, S.V., Bakaev, V.G., *et al.* (2006 a). Physical and technological issues of KrF laser drivers for inertial fusion energy. *J. Phys. IV France* **133**, 567-573.

Zvorykin, V.D., Ionin, A.A., Losev, V.F., Mikheevm, L.D., *et al.* (2006 b). Petawatt Excimer Laser Project at Lebedev Physical Institute. *AIP Conf. Proc.* **827**, 176-181.